



DEGREE PROJECT, IN NUCLEAR ENERGY ENGINEERING , SECOND LEVEL
STOCKHOLM, SWEDEN 2015

Identification of Silicon Phases in Highly Dense Uranium Nitride Pellets

PATRIK SIRÉN

KTH ROYAL INSTITUTE OF TECHNOLOGY
SCHOOL OF ENGINEERING SCIENCES

KUNGLIGA TEKNISKA HÖGSKOLAN

**Master in Nuclear Energy Engineering
Reactor Physics Department**

Master's Thesis



Identification of Silicon Phases in Highly Dense Uranium Nitride Pellets

Patrik Sirén

Supervisor:

Dr. Mikeal Jolkkonen, KTH, Sweden

Examinator:

Dr. Janne Wallenius, KTH, Sweden

Stockholm, Sweden, 2015

Abstract

In this thesis have impurity phases containing silicon located in highly dense uranium nitride pellets been identified. The pellets are manufactured with a new technique involving nitride powder and spark plasma sintering. Silicon arise in the pellets during the manufacturing process as an impurity and its impact on density has to be evaluated in order to permit assessment of measured thermal conductivity of the pellets. By using a SEM equipped with EBSD the phase was determined to $\text{Co}_3\text{Si}_5\text{U}_2$. However, EDS analyses revealed that most of the silicon is located in the bulk or in phases at the grain boundary, a result that gives no support to the hypothesis of silicon increasing the density by acting as a pore filler.

In an earlier study, the solubility limit of silicon in UN at 1500 °C got estimated to $(\text{UN}_{0.72}\text{Si}_{0.28})$ with a lattice parameter of 4.9003 Å. Since the examined pellet only contained around $(\text{UN}_{0.991}\text{Si}_{0.09})$ silicon, there is no surprise that we do not observe a shift of the lattice parameter in the bulk.

Combining these results gives the conclusion that, impact on density from silicon phases are negligible.

Acknowledgements

I will use this opportunity to thank everyone that helped me make this thesis possible.

First, I would like to thank my family, in particular my mother and father for their immeasurable support during these five years. Words cannot describe how thankful I am.

I'd also like to thank Kyle Johnson for all the help and support during the project, being an enjoyable and funny person is just a big plus. Kyle was also the one that carried out the manufacturing process, XRD analyses and calculated the theoretical density.

In addition, I'd like to thank Janne Wallenius and Mikeal Jolkkonen for giving me the opportunity to work with this project and for letting me use the Fuel lab.

To everyone in the lab: Kyle, Alicia and Mikael, I'd like to thank you all for all of the help you gave me and for the fellowship we shared.

I would also like to thank Oskar Karlsson at KIMAB, for operating their SEM and for letting me sit alongside when doing so.

Last, I'd like to thank all the great people at KTH that I have meet during these years, it has been a pure pleasure and I wish you all the best in the future.

Contents

Abstract	iii
Acknowledgements	v
List of Figures	ix
List of Tables	xi
1 Introduction	1
2 Tools and Methods	3
2.1 Manufacturing Method of Uranium Nitride	3
2.1.1 Setup of Equipment for Synthesis Process	3
2.1.2 Starting Material	4
2.1.3 Hydriding	4
2.1.4 Nitriding	5
2.1.5 Denitriding	6
2.1.6 Spark Plasma Sintering	6
2.2 Sample Preparation for SEM Analysis	7
2.3 Scanning Electron Microscope	11
2.3.1 Basic Components	11
2.3.2 Signal Detection	12
2.3.3 Microscopes and Analysis Software Used	13
2.4 Analysis	14
2.4.1 XRD & XRF	14
2.4.2 SEM	14
3 Results & Discussion	17
3.1 X-Ray Fluorescence & X-Ray Diffraction	17
3.1.1 X-Ray Fluorescence	17
3.1.2 X-Ray Diffraction	17
3.2 Scanning Electron Microscope	18
3.2.1 Philips XL-30 ESEM, KTH	18
3.2.1.1 SUN150225A4	18
3.2.1.2 SUN150302A5	23
3.2.1.3 SUN150302A1	25

3.2.1.4	SUPD140331A1	26
3.2.1.5	Discussion	28
3.2.2	LEO 1530, Swerea KIMAB	29
3.2.2.1	EDS	29
3.2.2.2	EBSD	34
3.2.2.3	Discussion	34
4	Conclusion	36
	References	37

List of Figures

2.1	Furnace for the synthesis process. Observe that the process is not running as the quartz tube is not inserted	4
2.2	Temperature and gas flow difference during hydriding of legacy uranium metal	5
2.3	Temperature and gas flow difference during nitriding of legacy uranium hydride powder	6
2.4	Typical appearance of manufactured uranium nitride pellets	7
2.5	Used mechanical polishing device	9
2.6	Used diamond lubricants, from left to right: 9 μm - 0.05 μm	9
2.7	Left: Medium hard woven silk cloth (9 μm to 1 μm). Right: Soft synthetic velvet cloth (0.25 μm to 0.05 μm).	10
2.8	VWR USC200TH ultrasonic cleaner, used to clean the pellets	10
2.9	Final result of sample preparation	11
2.10	The FEG-SEM equipment used at KTH	14
2.11	Phase diagram for U-Si	16
3.1	Obtained data from XRD analysis	18
3.2	Typical appearance of the sought silicide	18
3.3	Line scan over a silicide in the SUN150225A4 pellet	19
3.4	Obtained data from the line scan	19
3.5	Line scan over a silicide in the SUN150225A4 pellet	20
3.6	Obtained data from the line scan	20
3.7	Line scan over a silicide in the SUN150225A4 pellet	21
3.8	Obtained data from the line scan	21
3.9	Line scan over two silicides in the SUN150225A4 pellet.	22
3.10	Obtained data from the line scan	22
3.11	Line scan over a silicide in the SUN150302A5 pellet	23
3.12	Obtained data from the line scan	23
3.13	Line scan over a silicide in the SUN150302A5 pellet	24

3.14	Obtained data from the line scan	24
3.15	Line scan over cloud formed silicon phases in the SUN150302A5 pellet . .	25
3.16	Obtained data from the line scan	25
3.17	Line scan over a silicide in the SUPD140331A1 pellet	26
3.18	Obtained data from the line scan	26
3.19	Five point scans on the silicide	27
3.20	Pellet SUN150225A4 at Magnitude = 1000. Observe the now visible grain boundaries after etching with a 2% nital solution (ethanol and nitric acid) .	29
3.21	Ten point scans over an interesting region	30
3.22	An needle-shape phase located at the grain boundary, in close proximity to a 'chaotic' phase. Three point scans over the chaotic phase was done. . . .	32
3.23	Point scans on a silicide containing a darker phase on the tip of it	33
3.24	Interface of the AZtecEnergy software. To the upper left is the observed silicide and right to it is the kikuchi pattern. Below this pattern is the integrated MAD function, which display that Co ₃ Si ₅ U ₂ is the most likely phase	35

List of Tables

2.1	Manufactured pellets and their sintering parameters.	7
2.2	Measured and calculated density for the pellets	8
2.3	Physical density and calculated uranium density for the expected phases .	16
3.1	Obtained data from the point scans of an silicide containing four different phases	27
3.2	Data from ten point scans over an interesting region	31
3.3	Data from point scans of the chaotic phase	32
3.4	Data from point scans of an silicide	33

1 Introduction

In an age when it has never been more obvious that the electricity generation needs to be clean and safe, nuclear reactors are producing electricity at reasonable prices without creating any major carbon dioxide emissions that would influence the global climate. Nuclear power has, however, challenges to face e.g.: radioactive waste, potential accidents, nuclear proliferation and limited resources of U-235. In order to subdue these problems the nuclear power industry initiated in 2000, the Generation IV International Forum (GIF). It is an international corporation representing governments from 13 countries, set up to carry out the research and development needed to establish the feasibility and performance capabilities of the next generation nuclear energy systems [1]. About one hundred reactor technology concepts were reviewed and six of them were selected for further investigation. These selected concepts are clean, safe, reliable, cost-effective and use a closed fuel cycle to maximise the resource base and minimise high-level wastes to be sent to a repository [2].

There is a big difference between the six concepts in how they try to achieve this and parameters like: neutron spectrum, coolant, moderator, temperature, pressure, fuel and power of the reactor have different solutions from one concept to another. In the Reactor Physics Department at KTH, most of the research is focused on a concept called 'Lead-cooled fast reactors'. This concept is a nuclear reactor using high energy neutrons with lead or lead-bismuth as coolant. The fuel in this reactor is a nitride composition of Uranium-238 (with some U-235 or Pu-239) from depleted light water reactor fuel [2]. Before uranium nitride fuel can be used in a reactor, exact knowledge of its thermo-physical properties is required to assure a margin of failure, in case of an accident during operation.

A number of independent studies to determine the thermal conductivity have been made in the past. When correcting for as-manufactured porosity, the results between the studies shows a variation of up to 25% for the derived conductivity of a fully dense UN [3]. These deviations cannot distinctly be assigned to impurities nor stoichiometry [3-4]. An element that could influence the results is the porosity which varied from 2% to 7% in the measurements. With the purpose of removing this uncertainty, a manufacturing process producing highly dense uranium nitride pellets was crafted.

The manufacturing process consists of a synthesis procedure that combines hydriding and nitriding of metallic uranium and a spark plasma sintering (SPS) procedure. These techniques make it possible to manufacture a fully dense nitride pellet, with an average porosity of 0.2%. Elemental analysis of manufactured pellets revealed silicide phases, which arise during the synthesis procedure due to contamination from a

quartz filter in the furnace [3]. It's been assumed in previous studies that most of this silicon settles in pores as needle-shaped silicides during spark plasma sintering, thereby increasing density [5]. The exact impact of this has to be evaluated to permit assessment of measured thermal conductivity of the pellets.

The objective with the research presented in this report, has been to determine the phase of the silicide and examine the impact of using different parameters during SPS.

2. Tools and Methods

In this chapter, the manufacturing method and sample preparation of uranium nitride is reviewed. Understanding these steps are extremely important in order to do a correct analyse of the images produced in the scanning electron microscope. Furthermore a brief explanation on how the scanning electron microscope operates is given, followed by a walkthrough for how the analyse was performed.

2.1 Manufacturing Method of Uranium Nitride

The manufacturing process for produced uranium nitride pellets in this thesis is based on a method published by 'P.Malkki et al' in Journal of Nuclear Materials [3]. It uses a technique that differs greatly from the common manufacturing method [6]. The normal procedure to produce uranium nitride is by carbothermic nitriding. Some benefits with that method are usage of stable oxides as starting materials and major experience with handling oxide fuel. However, it also leads to large particles which requires milling to achieve a high density [3].

The synthesis method applied for this thesis instead follows a procedure by first hydriding and then nitriding the uranium. Using this procedure one gets a fine powder, for which no milling is required. By implementing the relative new spark plasma sintering technique, the powder is sintered into uranium nitride pellets. Advantages with this procedure compared to the more traditional sintering methods like, pressureless sintering or hot-pressing, is shorter production time and higher density of the pellet [7].

2.1.1 Setup of Equipment for Synthesis Process

The synthesis process is performed in a 25 x 1000 mm quartz tube, which is vertically mounted in a resistive heating furnace, see Figure 2.1. On the bottom end of the quartz tube is a gas mixer connected where the reaction gases are merged. Attached to the mixer are two gas lines, from which one of them hydrogen is injected. The other gas line can be shifted between injecting nitrogen or argon. To ensure low amount of impurities in the system, both gas lines are equipped with a gas cleaning system. The gases exit the systems from the top of the quartz tube where a filter system is installed, this prevent small particles to migrate into the ventilation system. The uranium metal is placed on a porous quartz filter at half height of the quartz tube, it is by contamination from this filter the sought silicon phase originate from.

To control & monitor the temperature and gas flows of the system, a K-type thermocouple and flow controllers is attached to the furnace and connected to a standard PC with the software LabVIEW installed. Using this software it is possible to

program a set of temperature and gas flow sequences for the furnace to automatically follow.

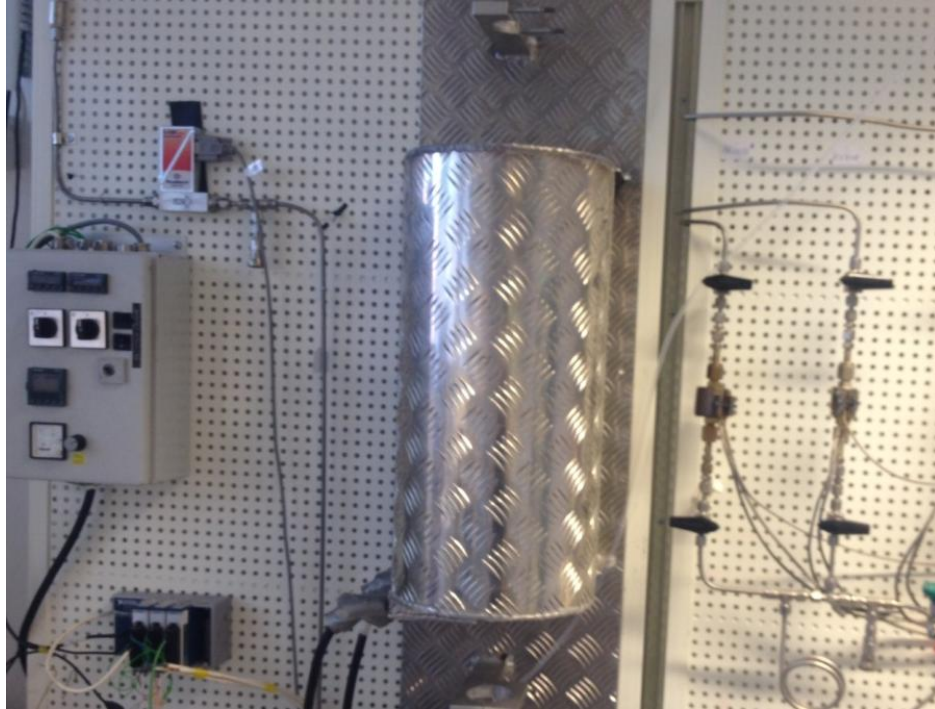


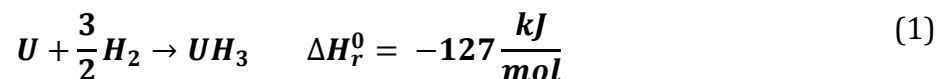
Figure 2.1: Furnace for the synthesis process. Observe that the process is not running as the quartz tube is not inserted.

2.1.2 Starting Material

Used uranium originates from two sources. The pellet manufactured in 2014 have depleted uranium derived from Oakridge material science. While Uppsala University provided with natural uranium for pellets manufactured in 2015. Since the uranium was not stored in a protective atmosphere, it got severely oxidized on the surface. To remove this oxide layer the uranium was grinded down until it had an oxygen content around 500-800 ppm. The uranium from both sources can be referred to as "legacy uranium".

2.1.3 Hydriding

By exposing the uranium metal to hydrogen at low reaction temperatures, uranium hydride (UH_3) is formed [3]:



During this process the volume increases significantly, causing the uranium hydride to spall off as fine powder and exposing fresh metal surface to the reaction. It is a continuous process until all metal has been converted into powder. Since no milling is required the risk of contaminate the sample with oxygen is substantially reduced.

The hydriding process was performed in a gas flow of 0.3 dm³/min H₂ and 0.1 dm³/min Ar. Using argon is merely a safety measure in case of back suction of air through the gas outlet. Which could lead to contamination of the sample or even worse,

a violent chemical reaction between hydrogen and oxygen [8]. Registered differences in gas flow and temperature are displayed in Figure 2.2. The initial temperature was set to 325 °C in order for the hydrogen to reach equilibrium. It is then lowered to 225 °C so the reaction could start. After around 14 000 s the gas flow difference is zero indicating that the process is complete.

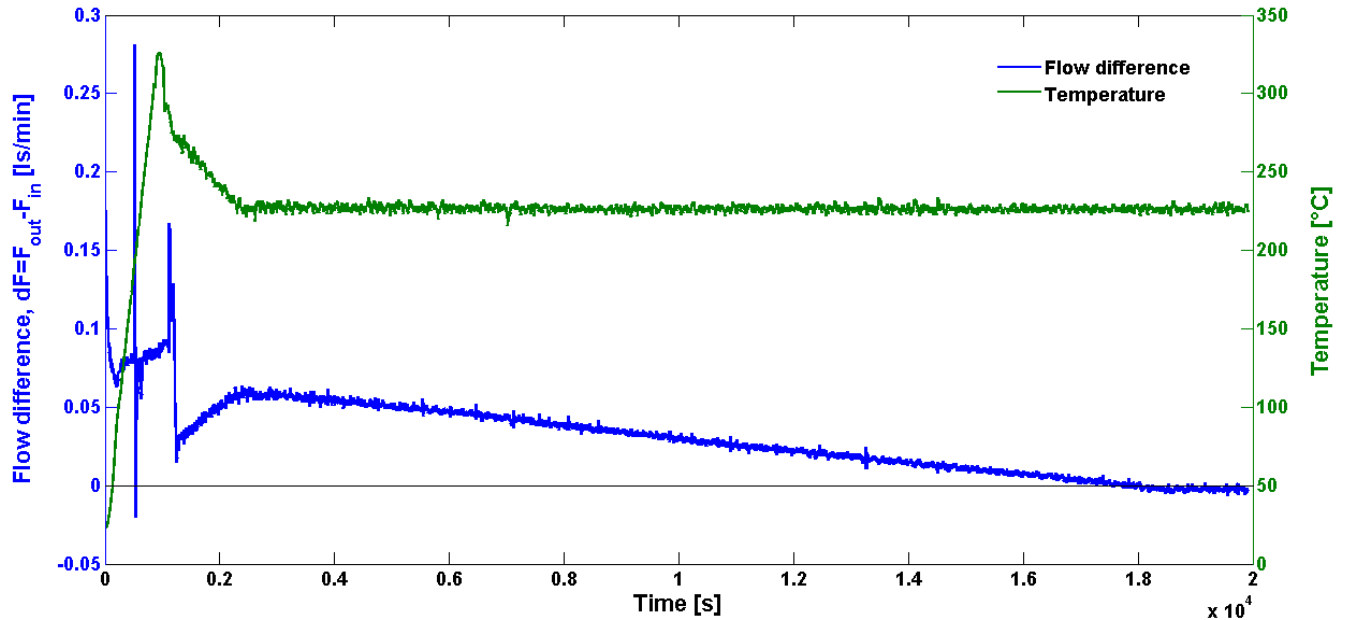
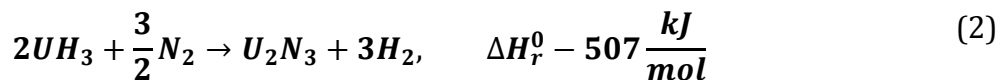


Figure 2.2: Temperature and gas flow difference during hydriding of legacy uranium metal.

2.1.4 Nitriding

The next step is nitriding the uranium hydride and can be performed directly after by introducing N₂ during an increase of temperature. The chemical exchange occurs according to equation (2) [3].



As displayed in Figure 2.3, the reaction is swifter than for the hydriding reaction. This is due to the product now being in powder form, providing a higher amount of surface area. The gas flow of the nitriding was set to 0.4 dm³/min N₂ and target temperature to 500 °C with a ramp of 10 °C/min. Around 400 s into the process, temperature dropped due to an insulation problem. This incident prolonged the procedure but it did not affect the end result. After 2175 s the nitriding was completed as temperature reached 500 °C with a stable gas flow difference.

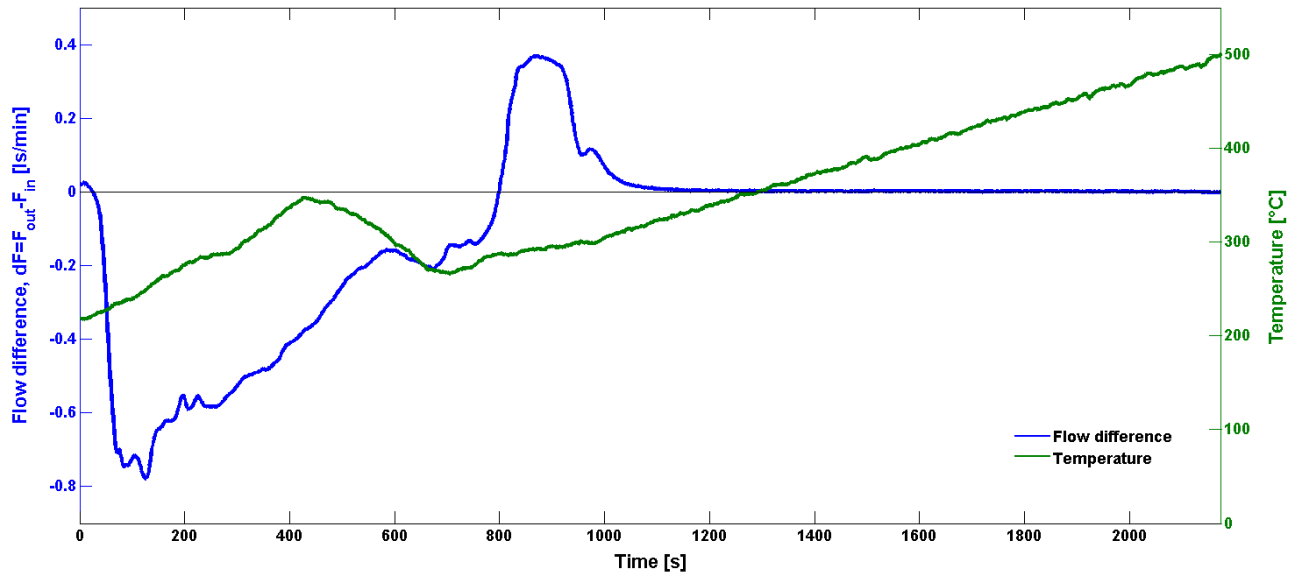
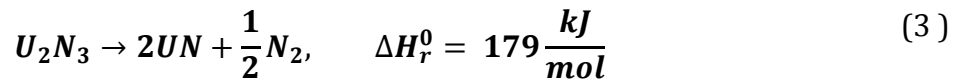


Figure 2.3: Temperature and gas flow difference during nitriding of legacy uranium hydride powder.

2.1.5 Denitriding

Uranium sesquinitride (U_2N_3) is thermally unstable. Using inert argon gas at $T \geq 1150\text{ }^\circ\text{C}$ decomposes it into the desired uranium mononitride (UN) according to equation (3) [3]:



The denitriding process was conducted directly after nitriding, with an argon flow rate of $0.3\text{ dm}^3/\text{min}$ and a temperature held at $1150\text{ }^\circ\text{C}$. It took 7.4 hours for the reaction to be completed. By using the optimal denitriding temperature of $1300\text{ }^\circ\text{C}$ the process could be quicker, but due to limitations of the quartz tube it was not possible in this project [3].

2.1.6 Spark Plasma Sintering

Sintering is a process where the powder is heated below its melting temperature. Allowing bonding to take place by diffusion of atoms, which lead to coalescence of powder particles into a more dense mass.

The method used in this thesis, spark plasma sintering (SPS) is a relative new technique which only takes a few minutes to complete. Powder for each sample is loaded into a cylindrical graphite die with graphite punches. The machine utilise a high electrical DC pulse between graphite electrodes to heat the sample. This combined with pressure gives a higher densification at a shorter time compared to conventional sintering methods. Heating rates up to $1000\text{ }^\circ\text{C}/\text{min}$ is achievable with SPS [3,7].

A total of four pellets were manufactured using this technique, where three variables: time, pressure and temperature varied for each sample according to Table 2.1.

Table 2.1: Manufactured pellets and their sintering parameters.

Pellet	Time (min)	Pressure (kN/cm ²)	Temperature (°C)
SUN150225A4	15	10	1650
SUN150302A1	15	15	1450
SUN150302A5	3	14.8	1650
SUPD140331A1	15	5	1450

A typical sintered uranium nitride pellet can be seen in Figure 2.4. Having a dark gray metallic color.



Figure 2.4: Typical appearance of manufactured uranium nitride pellets.

2.2 Sample Preparation for SEM Analysis

Sample preparation is a key step for scanning electron microscope analysis (SEM). With more than 90% of the problems associated with image analysis originated from a careless preparation, the biggest challenge is obtaining the required image quality to the microscope. Performing a thorough and proper preparation can be the difference between getting useful data from the SEM analysis and getting no information at all, "garbage in, garbage out" [9].

The first measure during the preparation is to remove carbon residues on the pellets crust that appeared during sintering. Using silicon carbide paper (SiC) P320, the surface is manually grinded down until a visible difference could be seen. To prevent grinded powder from become airborne, paraffin oil was used as lubricant.

Density

Next step was to determine actual porosity of pellets by using Archimedes' principle. The principle utilises that there is a relation between the volume of an object to the mass of liquid displaced when the object is immersed therein. Mass of each pellet got

measured before submerged into a cup of chloroform. The cup was then placed in a vacuum chamber with a pressure just above the vapor pressure for chloroform, and stored there until to no visible traces of air escaping from the pores could be seen, indicating a complete absorption of the chloroform into the pores. The mass was then measured again and by inserting these values into equation 4, the density could be calculated.

$$\rho = \frac{m_{\text{pellet}} * \rho_{\text{chloroform}}}{m_{\text{pellet}} - m_{\text{chloroform}}} \quad (4)$$

Where the density of chloroform is taken as 1.483 g/cm³.

The theoretical density can be estimated by measuring the: oxygen, nitrogen, carbon and silicon amount in the pellet and using mol calculations. Exact procedure is out of scope for this text, but the result is to a small extent dependant on which phase the silicon is in. If exact knowledge of this phase is known the theoretical density can be determined more accurately.

The theoretical density is an estimation in which there is no pores in the pellet, so by dividing measured density with calculated theoretical density, a relative density is given. The value of this relative density is a clear indicator of how dense the pellet is, where 100% is a fully dense pellet with no pores. Density of the pellets is displayed in Table 2.2, where the silicon phase for the theoretical density is for now assumed as U₃Si₂.

Table 2.2: Measured and calculated density for the pellets.

Pellet	Density (g/cm³)	Theoretical density (g/cm³)	Relative density (%)
SUN150225A4	13.87	14.27	97.20
SUN150302A1	12.16	14.27	92.52
SUN150302A5	13.60	14.27	95.30
SUPD140331A1	12.80	14.27	89.96

Mounting

For easier handling during sample preparation and in order to optimise material usage, the pellets got shattered into smaller pieces and the most suitable one from each pellet got selected for compression mounting. To be classified as a suitable piece it should not have been damaged during the shattering. Pieces with cracks and highly stressed areas were avoided.

During compression mounting the piece is encapsulated with bakelite powder under heating and pressure. This simplifies handling of the sample and protect outer edges during preparation steps. An important arrangement during mounting is the placement of the piece, as it should be positioned so the most interesting surface is shown.

Grinding & Polishing

To retrieve the partial hidden piece after mounting, a part of the bakelite had to be grinded off. This was done by once again use SiC paper with grit designation P320. After some minutes of grinding the whole surface could be seen. Next step is to remove sectioning effects and establish a flat surface. This was achieved by using gradually finer SiC papers (P600 P800 P1200). As the depth of damage decrease with abrasive size and each operation removes the damage introduced from the previous one, a planar surface is obtained with this procedure.

The final step required to produce a scratch and deformation-free surface with mirror reflection is to polish the sample. For this a mechanical polishing device was used, see Figure 2.5.



Figure 2.5: Used mechanical polishing device.

The setup involved usage of diamond lubricants on a cloth. The cloth is attached to a rotating wheel and held in place using an adjustable clamp. Rotational speed of the wheel is adjustable with a max rpm of 3000. By applying diamond lubricant and smoothly pressing the pellet down into the cloth a shiny surface occurred. A similar approach as when grinding was applied, using five diamond lubricants with different grain size ($9\mu\text{m}$, $3\mu\text{m}$, $1\mu\text{m}$, $0.25\mu\text{m}$ and $0.05\mu\text{m}$), see Figure 2.6.



Figure 2.6: Used diamond lubricants, from left to right: $9\mu\text{m}$ - $0.05\mu\text{m}$.

Since cloths are manufactured to be optimal for certain grain sizes, two different cloths were used, see Figure 2.7. A medium hard woven silk cloth was used for lubricants with grain sizes from 9 μm to 1 μm . From 0.25 μm to 0.05 μm grain sizes, a cloth with soft synthetic velvet with low nap was used.

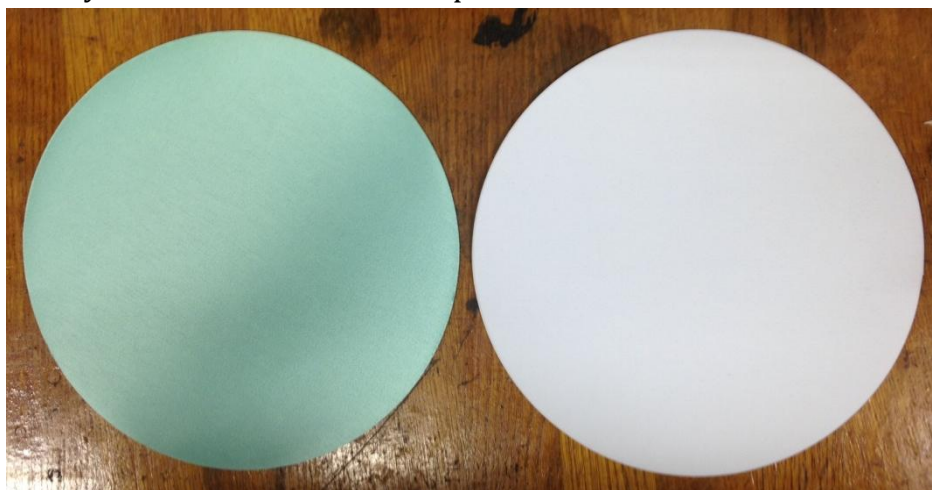


Figure 2.7: Left: Medium hard woven silk cloth (9 μm to 1 μm). Right: Soft synthetic velvet cloth (0.25 μm to 0.05 μm).

Cleaning

In previous studies it was discovered that dirt and aluminum, originated from the diamond lubricants got detected in the SEM [5]. Therefore, the last preparation step was to ultrasonic clean the pellets. This was done by placing the pellets in a glass with 99.5% ethanol and insert it into a VWR USC200TH filled with water, see Figure 2.8. Ultrasound with a frequency of 45 kHz then cleaned the pellets for 20 min.



Figure 2.8: VWR USC200TH ultrasonic cleaner, used to clean the pellets.

Final result of the sample preparation can be seen in figure 2.9.



Figure 2.9: Final result of sample preparation.

2.3 Scanning Electron Microscope

The scanning electron microscope is the most widely used type of all electron microscopes [10]. It was developed mainly because of the limitations that optical microscopy has. An optical microscopy has two major inherent limitations compared to the SEM. One being that the wavelength of visible light is broader than for electrons, providing images with lower resolution. The second limitation is the large aperture angle which is decreasing the depth of field.

Not constrained with these limitations the SEM can produce images of higher quality, however, electrons provide some limitations of their own. First of all, in air electrons will quickly disperse or scatter due to collisions with other molecules, therefore, the equipment and sample must be under vacuum. Another limitation arise due to the electrically charge that electrons has, this requires the sample to be conductive in order to dissipate the charge [11].

2.3.1 Basic Components

The electrons which probe the sample in SEMs originates from an electron gun. A wide variety of electron guns exists, but the basic design is similar. One of the most common gun is the thermionic gun where the electrons are extracted from a heated tungsten filament. When heated an electron cloud forms around the filament. By placing an anode plate near the filament the negatively charged electrons are attracted towards it, and the electrons can be transported away from the filament. To prevent that the electrons jumps over to the anode plates, a cathode plate is also placed near the filament. This is the basic of an electron gun, having electrons travel through a hole in the anode & cathode plate, with a speed controlled by the amount of potential applied to the cathode and anode plates, typically in the range of 1-40 kV.

The electrons leaves the hole in a spray pattern. To control the flow of electrons and focus them into a beam, a series of column mounted electromagnetic lenses are used. The first lenses in the column is the condenser lenses, they control the size of the beam by regulate the number of electrons travelling through the column. Optimal size of the beam is a compromise between getting a better signal to noise ratio but lower resolution with larger beam diameter. The objective lens focuses the beam at a spot on the sample which is necessary to get a proper focus on the image.

In order to get the beam to scan across (map) the sample in an x-y raster, two electromagnetic scanning coils are included in the column. One will position or deflect the beam in x-direction, while the other does the same in y-direction. The scanning coils are controlled by a scan generator which regulates the current flowing in the coils, thus control the strength and direction of the beam deflection [12].

With this we have an electron beam that can map across the surface of our sample. But to form an image we need one more important component, the detector. In the next section (2.3.2) a more through explanation on how the signal detection works in a SEM is given, but simply put, electrons that interact with the sample will scatter and hit the detector. This signal is amplified and an image can be produced on a computer monitor. Since the electrons have a low travel distance in air, a vacuum chamber is connected to the system to ensure that the electrons reach the sample and detector [11,13].

2.3.2 Signal Detection

When a high energy electron reaches the sample three things can occur. First, the electron can pass through the sample. Second, it can collide inelastic with electrons from the inner shell of the sample and transfer enough energy to knock them out as free electrons. A knocked out electron is called a secondary electron (SE). Third, it can elastic collide with the nucleus of the sample and deflect out as a backscattered electron (BSE).

However, these are not the only particles being ejected from the sample. As the SEs are knocked out they leave holes in the electron shell and the atom becomes ionized. This is an excited state that is unstable, so the atom will quickly return to its normal state by letting electron from the outer shell fill the vacancy. The energy difference between an outer shell electron and an inner shell will generate a photon (Characteristic X-rays). By using an Energy Dispersive Spectroscopy (EDS) detector to analyse the energy of this photon, it is possible to evaluate the elemental composition of the sample.

To determine the crystallographic phase an Electron Back-Scatter Diffraction (EBSD) detector can be used [11,14].

Secondary Electrons

The SEs has a very low energy and therefore travels a short distance in the sample (5-50 nm). Thus this detection mode is used for the detector if topographical surface contrast is of interest. The contrast is formed by two effects, the trajectory effect and the electron number effect. The trajectory effect emerge from variations in how the sample surface is oriented with respect to the detector, which is similar for a light microscope. The electron number effect will produce light or dark areas depending on the shape of the surface. A hole in the surface will reduce the amount of electrons reaching the detector and a dark spot will be seen on the image. Whereas a hill will increase the number and a bright spot occurs [11,15].

Backscattered Electrons

The high energy of BSEs let them escape from deeper depth of the sample (50-300 nm), thus this detection mode give useful information about the elemental composition contrast of the sample. For BSE the contrast arise because of the number of backscattered electrons emitted from the sample increase with the atomic number. So areas with atoms of higher atomic numbers will appear brighter on the image [11,15].

Energy Dispersive Spectroscopy

Every atom has unique characteristic X-ray excitation energy. Using a Si(Li) detector the EDS system can collect these over a selected area and send the data to a computer software that creates a spectrum, where existing elements is shown as a peak in the spectrum.

By calculating the area under the peak the atomic fraction for each element can be estimated. The strength of using EDS is that one obtains elemental analysis at the same time as examining the microstructure of the material. Limitations are that: elements of low atomic number ($Z < 11$) cannot be properly analysed, and there is a detection threshold around 1000 ppm (0.1 wt.%) [11,15].

Electron Back-Scatter Diffraction

The principle of EBSD is that back-scattered electrons diffract against the crystal planes in the focal point of the electron beam. The diffraction pattern, Kikuchi pattern, is captured by the EBSD detector, consisting of a phosphorus screen with a CCD camera at the back side. The pattern is sampled, corrected for background and noise and then formatted with a computer image analysis system in order to obtain crystallographic phase and orientation [16].

2.3.3 Microscopes and Analysis Software Used

Two different scanning electron microscopes were used in this thesis. One belongs to the division of surface and corrosion science at KTH and the other one to Swerea KIMAB.

The used FEG-SEM equipment at KTH (see Figure 2.10) was a Philips XL-30 ESEM equipped with a 20 mm² Silicon Drift Detector (SSD) from Oxford Instruments. Used

SEM settings were 15 kV with an aperture of 120 μm . To analyse obtained data, the software INCA Energy from Oxford Instruments was used.

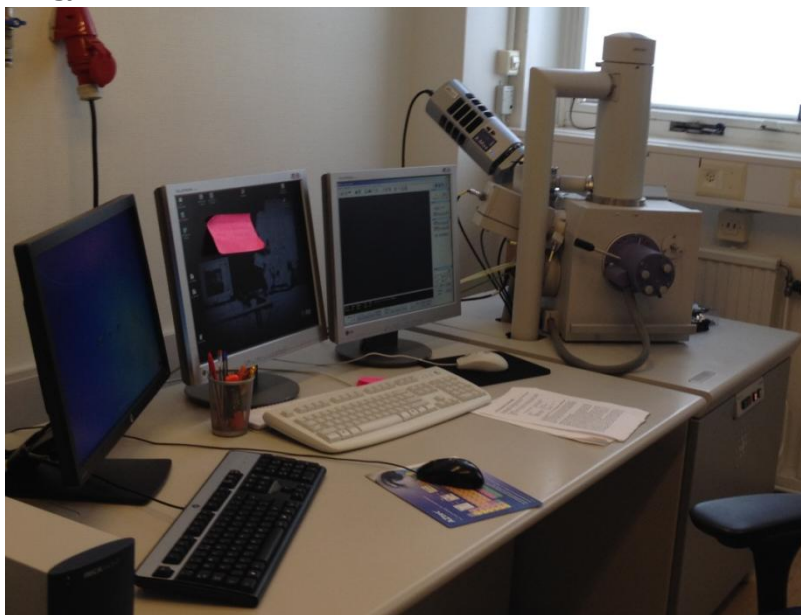


Figure 2.10: The FEG-SEM equipment used at KTH.

The used FEG-SEM equipment at Swerea KIMAB was a LEO 1530 with Gemini column, upgraded to a Zeiss Supra 55 (equivalent) with Channel 5 software from HKL Technology and a Nordlys F+ EBSD camera. The EDS detector was a 50 mm² X-Max Silicon Drift Detector (SDD) from Oxford Instruments. The SEM settings used was 15 kV with an aperture of 120 μm . Used EBSD settings was step size 0.5 μm (1000x), 0.05 μm (10000x) and 4x4 binning. To analyse obtained data, the software AZtecEnergy from Oxford Instruments was used.

2.4 Analysis

2.4.1 XRD & XRF

X-ray diffraction (XRD) measurements was made using a Siemens D5000 X-Ray Diffractometer, equipped with Cu k-alpha target at 40 mA and 35 kV voltage. Obtained spectra got benchmarked using EVA evaluation software in order to identify phases present. To identify trace elements, powder got sent to Degerfors Laboratorium for X-ray fluorescence (XRF) analysis, using a Thermo ARL 9800 instrument with an estimated relative error of 10 ppm [3].

2.4.2 SEM

After sample preparation the pellets were ready to be analysed in the SEM. Since the mounted bakelite is non-conductive, a carbon tape had to be attached on the back of the pellet before inserting it into the microscope chamber. Vacuum was applied and the: working distance, brightness and contrast were adjusted until a good image could be seen on the monitor.

Since main focus were to analyse elemental composition and mainly silicon phases, the BSE detection mode was used for the detector. In previous studies [3,5] it was observed that silicon often appeared as uranium silicide in needle-shaped phases. It was assumed that these silicides fill up pores during the spark plasma sintering process and hence increasing density of the pellets. Potential phases of the uranium silicides can be found from the phase diagram of U-Si, see Figure 2.11. Phases of interest are: USi, U₃Si, U₃Si₂ and U₃Si₅. As a first attempt to determine the exact phase an EDS detector was used to analyse elemental composition. This method utilises that intensity of the signal strength is proportional to amount of the element [5]. By performing line and point scans over the UN bulk and silicide to measure intensity changes, it should possible to determine uranium density in the silicide and thereby estimate the phase (if uranium density in the UN and silicide phases is known).

The uranium density in UN is determined to be 13.5 g/cm³ by equation 5:

$$\rho_{UN} = \frac{\rho_{UN} * A_U}{A_U + A_N} \quad (5)$$

Where ρ_{UN} is the density of UN inserted as 14.3 g/cm³, A_U and A_N are the atomic mass of uranium (238.02891 amu) and nitrogen (14.0067 amu), all values found on web elements [16].

Same calculations was done for all the possible silicon phases using: $\rho_{USi} = 10.96 \text{ g/cm}^3$, $\rho_{U_3Si_2} = 12.2 \text{ g/cm}^3$, $\rho_{U_3Si_5} = 9.06 \text{ g/cm}^3$ and $A_{Si} = 28.0855 \text{ amu}$. With results displayed in Table 2.3.

This procedure is a continuation from the previous research [5] and contains several uncertainties since the detected elemental concentration is not completely reliable. For example are elements of low atomic number like: nitrogen, oxygen and carbon overestimated compared to uranium and silicon.

The plan in this thesis was reduce this uncertainty by getting a good amount of data, trough scanning several silicides in each pellet. This data could possible determine if any potential phase is over representative in the pellets and if there is any difference depending on: time, pressure and temperature during the SPS process.

As the results appeared to have: deficiencies, being inconsistent and there was a misunderstanding about the functionality of the SEM (explained more thorough in chapter 3), it became obvious that this procedure would not be enough to determine the phase. To get around this problem we used a better SEM, equipped with an EBSD detector.

Table 2.3: Physical density and calculated uranium density for the expected phases.

Phase	Physical density (g/cm ³)	Uranium density (g/cm ³)	Change in respect to UN (%)
UN	14.3	13.5	-
USi	10.96	9.8	-27
U ₃ Si ₂	12.2	11.3	-16
U ₃ Si ₅	9.06	7.5	-44

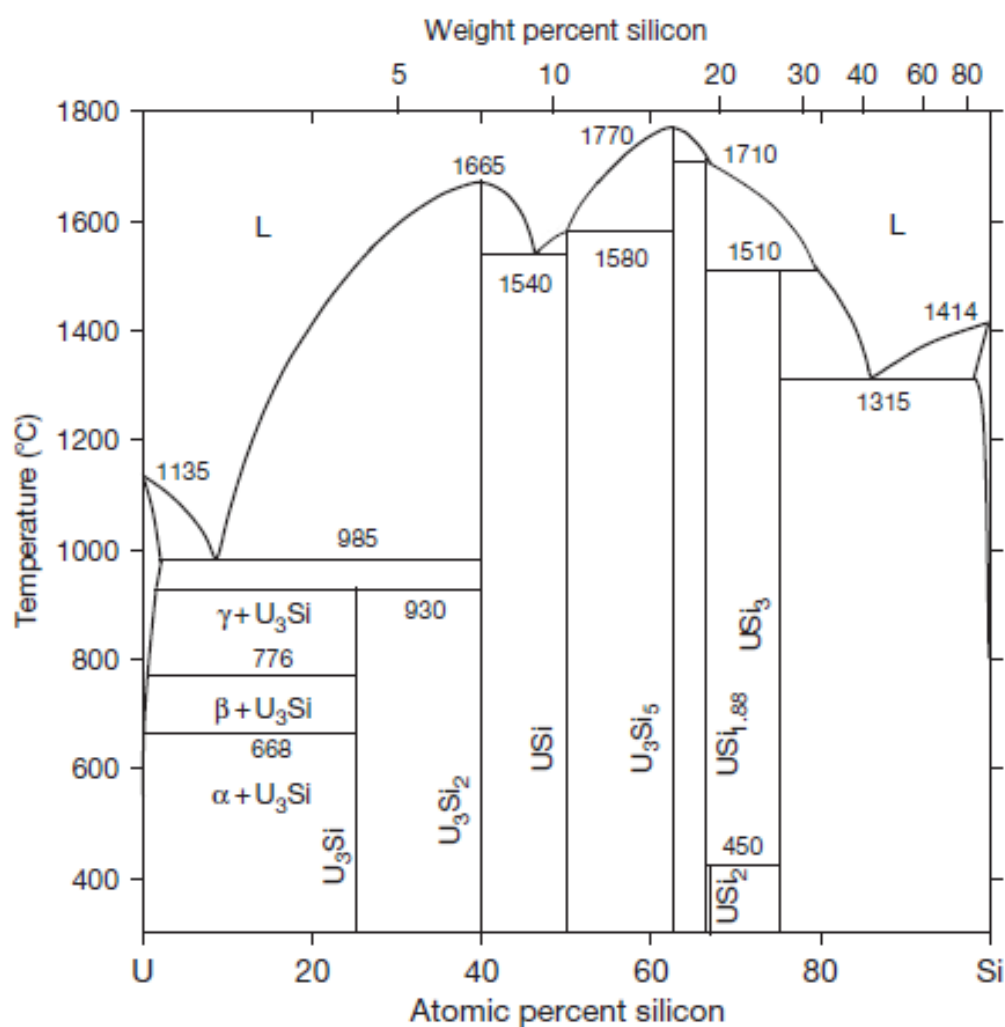


Figure 2.11: Phase diagram for U-Si [17].

3. Results & Discussion

In this chapter, all the results from the analysis will be presented. The chapter is divided into two separate sections. First section briefly presents results obtained from the XRD & XRF analyse. The second section presents and discuss results from the SEM analyse.

3.1 X-Ray Fluorescence & X-Ray Diffraction

In this section are results from the XRD and XRF analyses presented. These analyses are of importance since they could give a first indication of possible phases and trace elements in the pellets.

3.1.1 X-Ray Fluorescence

Powder from several pellets were examined with XRF analyse at Degerfors. Out of these contained pellet UPD140331 the highest amount of silicon content with 0.16 wt.%, while the lowest pellet had 0.06 wt.%. Other detected trace elements were: titanium, copper, iron and tungsten. Content of these elements varied between 0.05-0.19 wt.% depending on pellet. The analyse indicated that over 99 wt.% is uranium, which is clearly incorrect as around 5 wt.% should be nitrogen. This can simply be explained since XRF have similar limitations as the SEM with detecting light elements [19]. It is also the reason why it fails to detect carbon and oxygen, which instead got measured to 0.22 wt.% respectively 0.49 wt.%, using inert fusion gas instrument.

Detection limit depend upon the specific element and matrix of the pellet, where heavier elements usually have a better detection limit. The lowest detectable concentration appeared to be around 0.05 wt.%.

3.1.2 X-Ray Diffraction

The XRD analysis indicated only a cubic phase of uranium mononitride (UN), see Figure 3.1, implying that the manufacturing process succeeded. As no silicon phases got detected, the analysis is of no assistance in order to identify the silicides. This result was expected since the pellets only contain around 0.05-0.16% silicon and the detection limit is around 2 wt.% for XRD analysis [19]. Phases below this limit is usually clouded in the background noise. Also, if this low amount of silicon would happen to be present in different phases, it would be even harder to detect them in XRD analyse.

As the XRF and XRD analyses could not determine the phase of the silicide, focus got shifted towards SEM analyse.

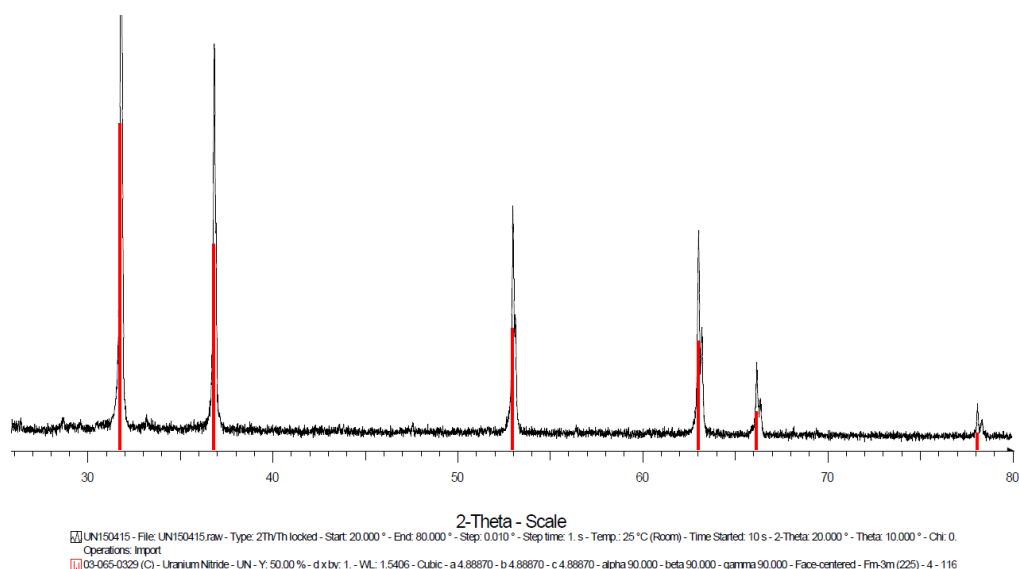


Figure 3.1: Obtained data from XRD analysis.

3.2 Scanning Electron Microscope

In this section are results from the SEM analyse presented. It is divided into two subsections, the first one introduces results from EDS analysis produced with the SEM available at KTH. In the second one, are results from EBSD and EDS analysis produced at Swerea KIMAB presented. At the end of each subsection is a short discussion about the results given.

3.2.1 Philips XL-30 ESEM, KTH

3.2.1.1 SUN150225A4

The first examined pellet was SUN150225A4. This is the most dense pellet which is favourable since less pores makes the needle-shape easier to find, as it stand out more from the bulk. Several silicides were found and line scans was performed to analyse elemental composition. The distinct needle-shape appearance of the silicide can be seen in Figure 3.2.

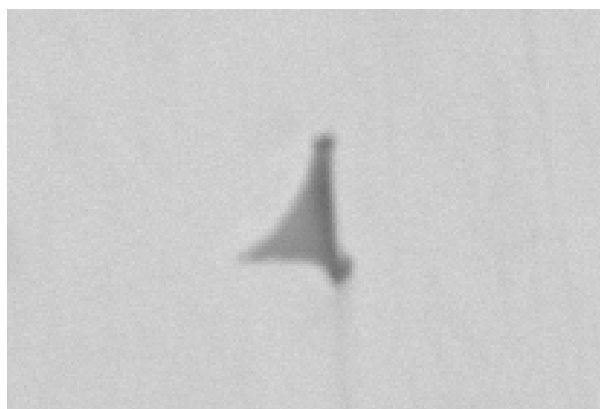


Figure 3.2: Typical appearance of the sought silicide.

A line scan over the silicide revealed an increase of silicon density and a deep drop of uranium and nitrogen density, see Figure 3.3-3.4. The intensity change for uranium is around -43% which could correspond to the U_3Si_5 phase, according to Table 2.3. In all analysis are carbon concentration disregarded, since the coating material (bakelite) is made of carbon which distort the measurement. To the upper left of the silicide is an oxygen impurity detected.

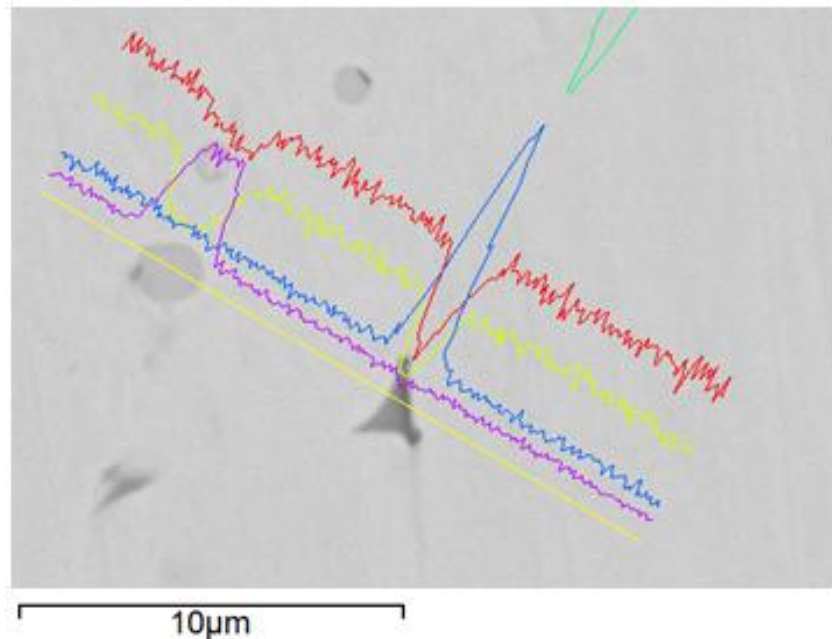


Figure 3.3: Line scan over a silicide in the SUN150225A4 pellet.

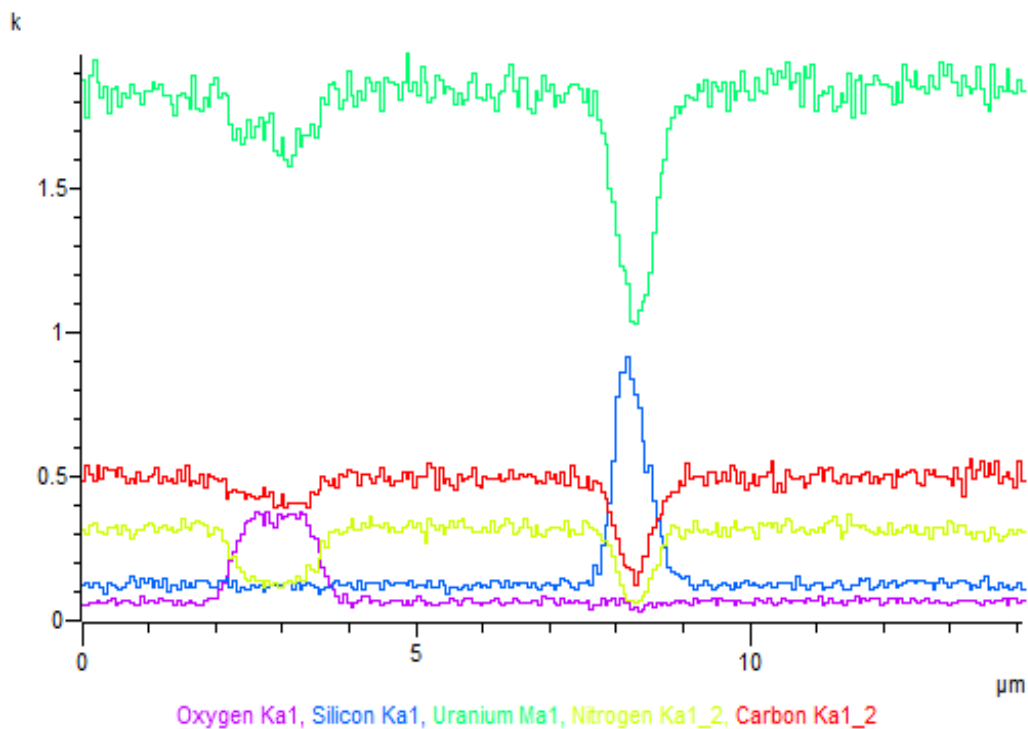


Figure 3.4: Obtained data from the line scan.

Similar results for another silicide is seen in Figure 3.5-3.6. There is an intensity change of uranium by around -38%, which as well indicate the U_3Si_5 phase. The EDS analyse also revealed iron, this was not something unique for this silicide. But usually the small amount of detected iron was overlooked as unimportant and perhaps being an issue with overlapping energy peaks and therefore disregarded from the scans.

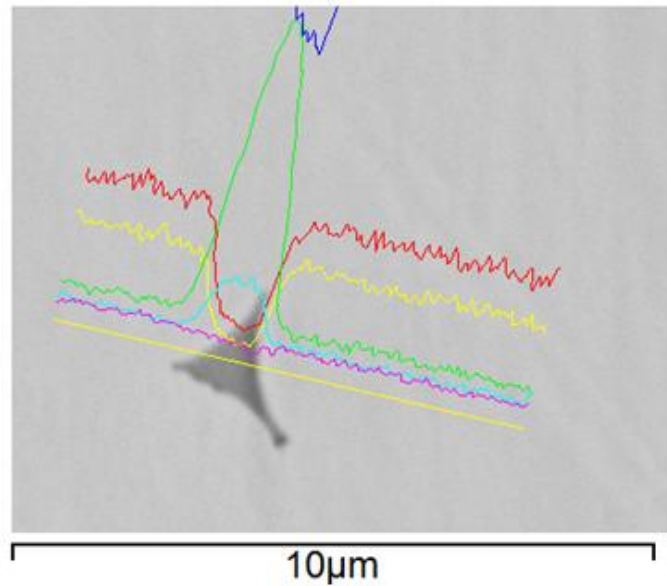


Figure 3.5: Line scan over a silicide in the SUN150225A4 pellet.

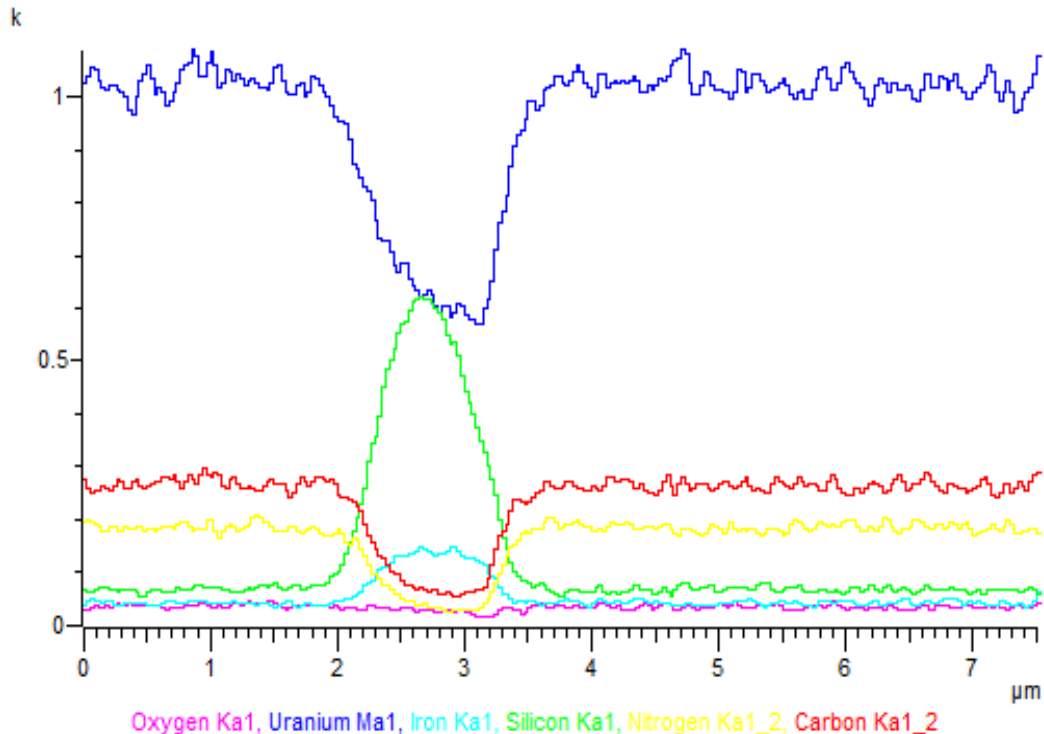


Figure 3.6: Obtained data from the line scan.

Occasionally the silicide consisted of two different phases, one example can be seen in Figure 3.7-3.8. The dark phase appear to be captured inside the brighter one and assemble around the corners of the triangle. A remarkable note is that detected silicon counts is higher than for uranium. The intensity change of uranium is around -80%, this does not correspond to anyone of the expected phases. Another notation is the high intensity of molybdenum, which most likely belong to the darker phase.

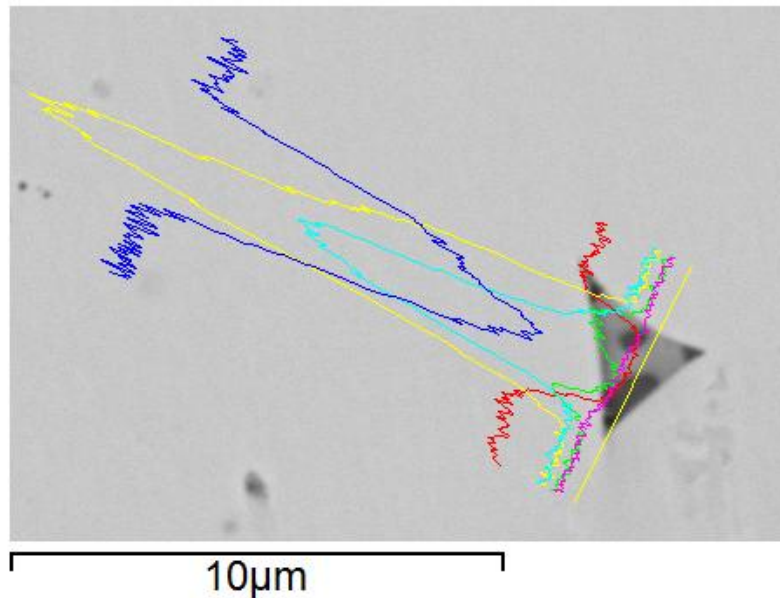


Figure 3.7: Line scan over a silicide in the SUN150225A4 pellet.

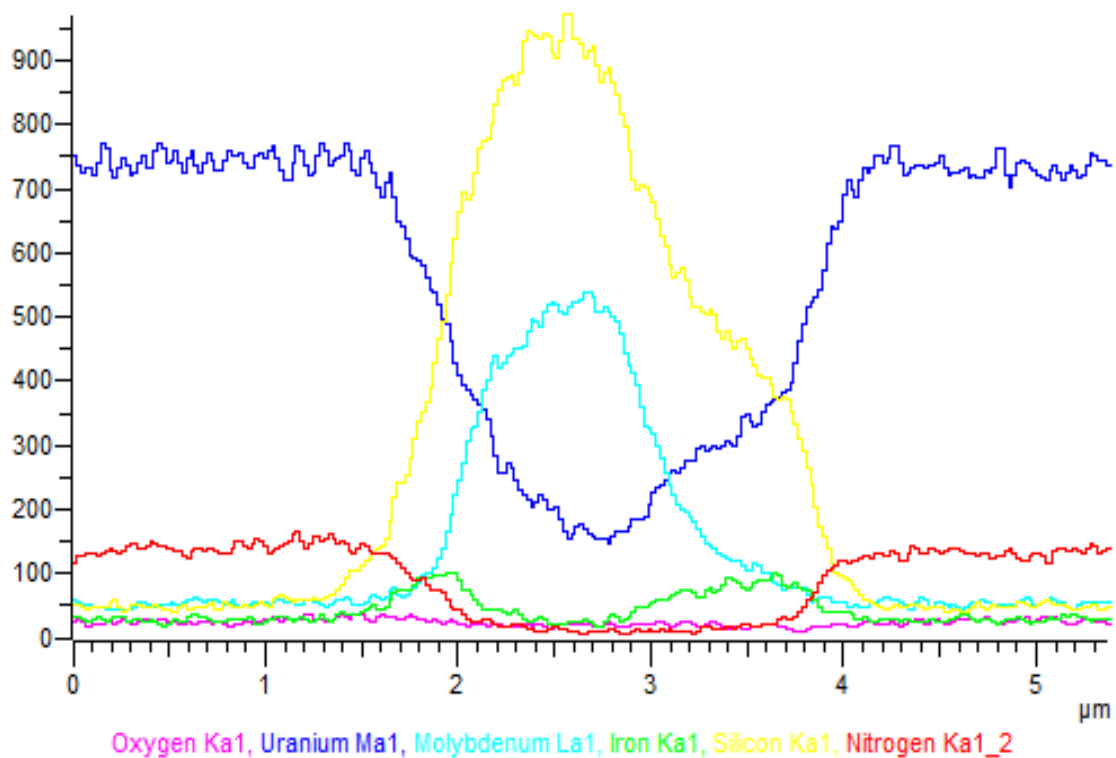


Figure 3.8: Obtained data from the line scan.

A more rare case where two silicides are positioned close to each other was analysed, see Figure 3.9-3.10. The right silicide have a intensity change of uranium around -42% which once again could correspond to the U_3Si_5 phase, while the left silicide had a change around -35% which makes it more uncertain since the value is between the USi phase and U_3Si_5 .

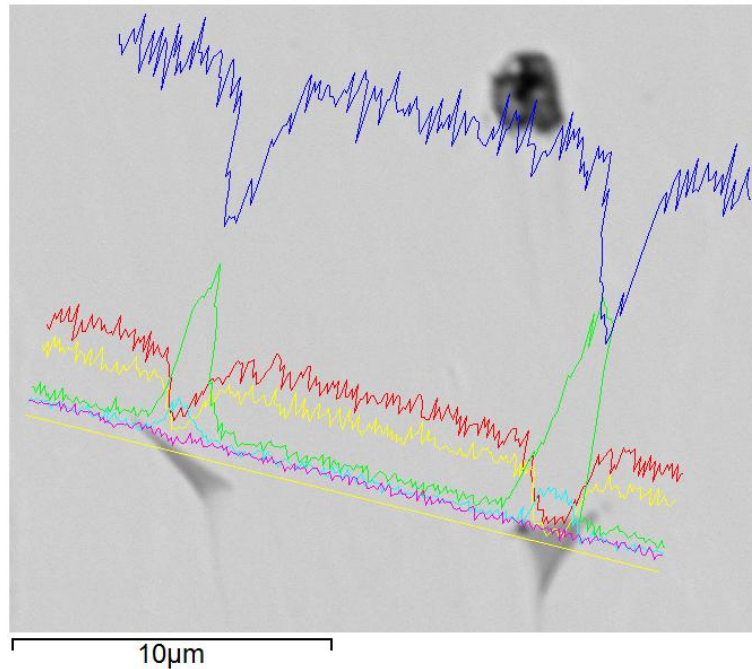


Figure 3.9: Line scan over two silicides in the SUN150225A4 pellet.

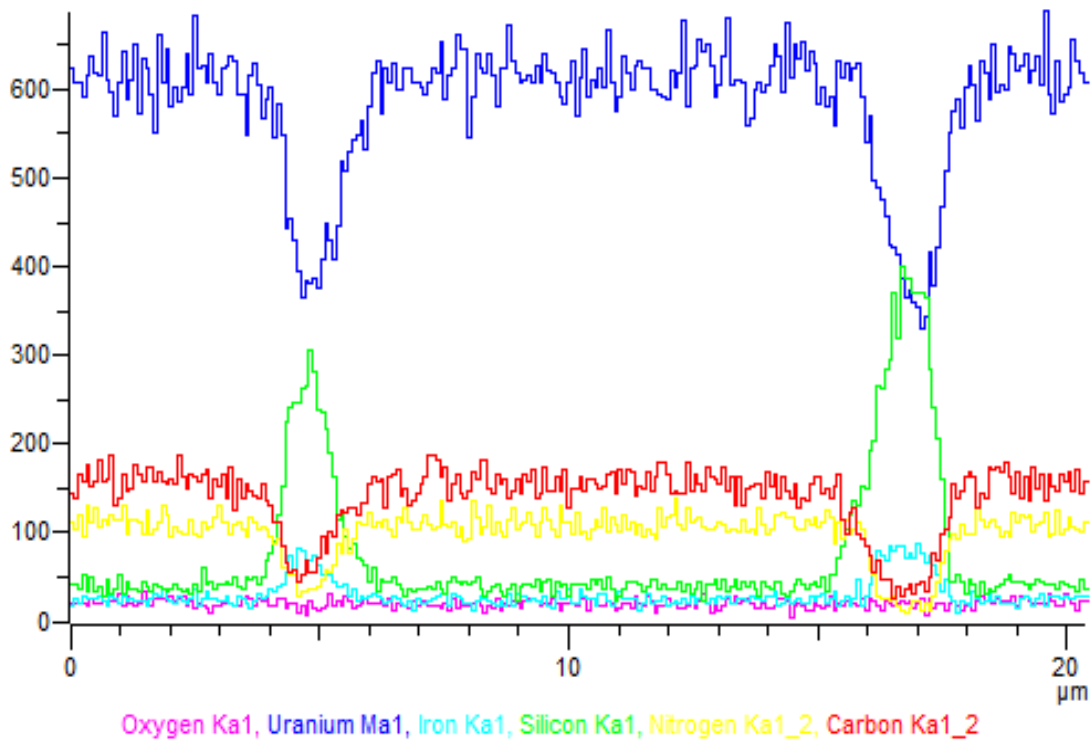


Figure 3.10: Obtained data from the line scan.

3.2.1.2 SUN150302A5

This pellet was manufactured with the shortest sintering time and a high pressure. Characteristic results from a line scan can be seen in Figure 3.11-3.12. The uranium intensity drop is around -25%, revealing a possible USi phase. Compared to SUN150225A4 the intensity drop of uranium appeared to be lower. A small amount of the trace elements: cerium and fluorine was also detected.

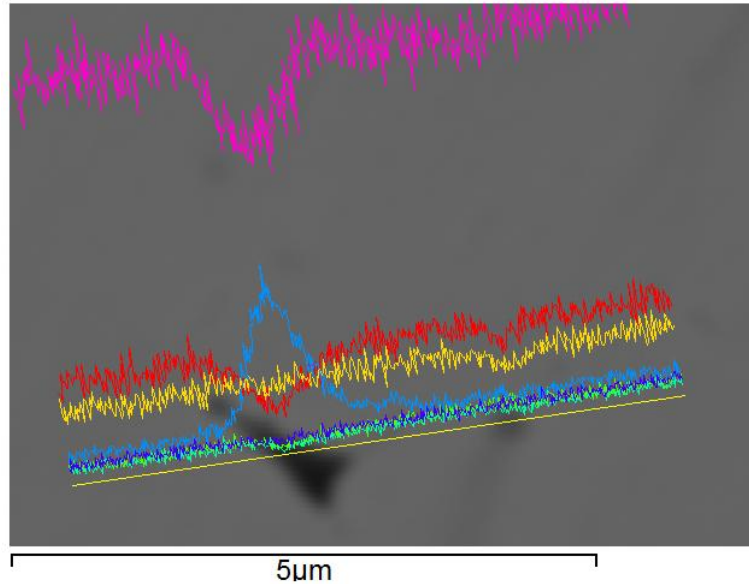


Figure 3.11 Line scan over a silicide in the SUN150302A5 pellet.

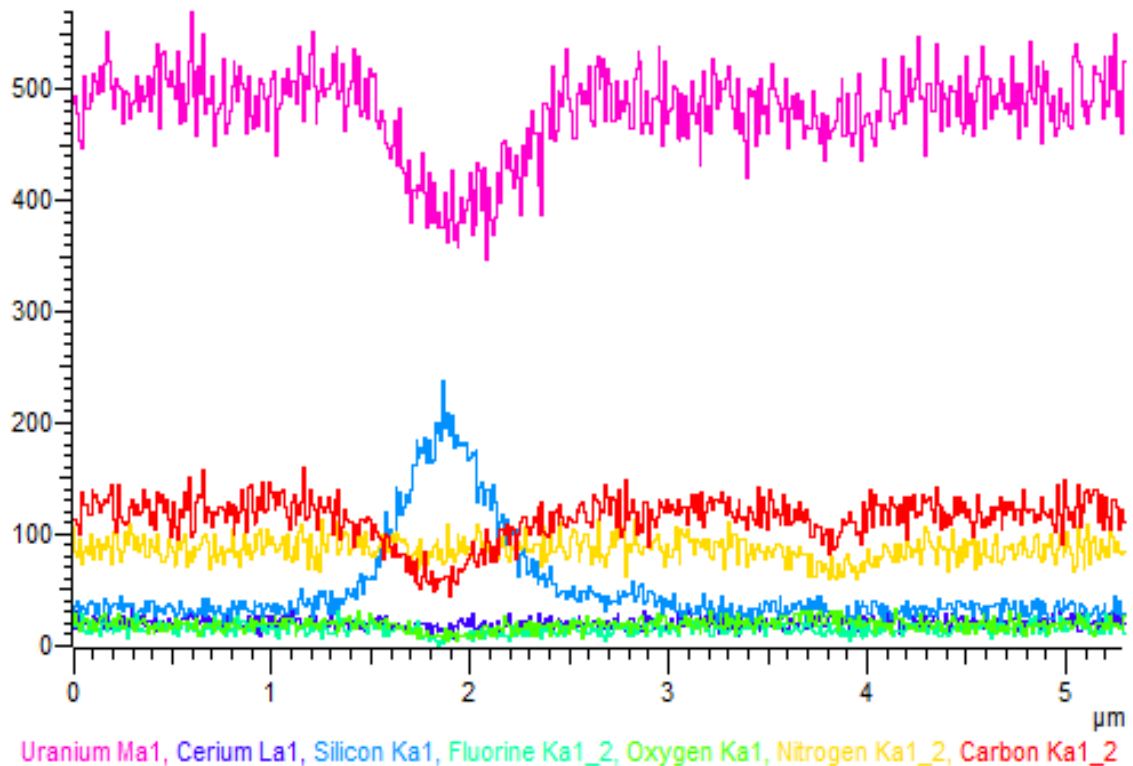


Figure 3.12: Obtained data from the line scan.

Similar results are detected in the silicide seen in Figure 3.13-3.14. With uranium intensity change around -26% and an oxygen impurity seen on the right side.

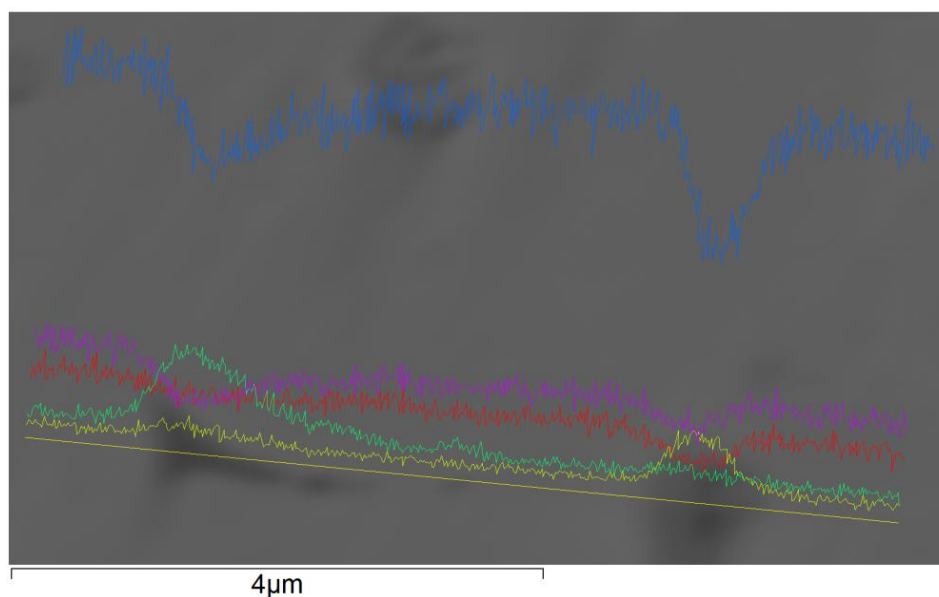


Figure 3.13: Line scan over a silicide in the SUN150302A5 pellet.

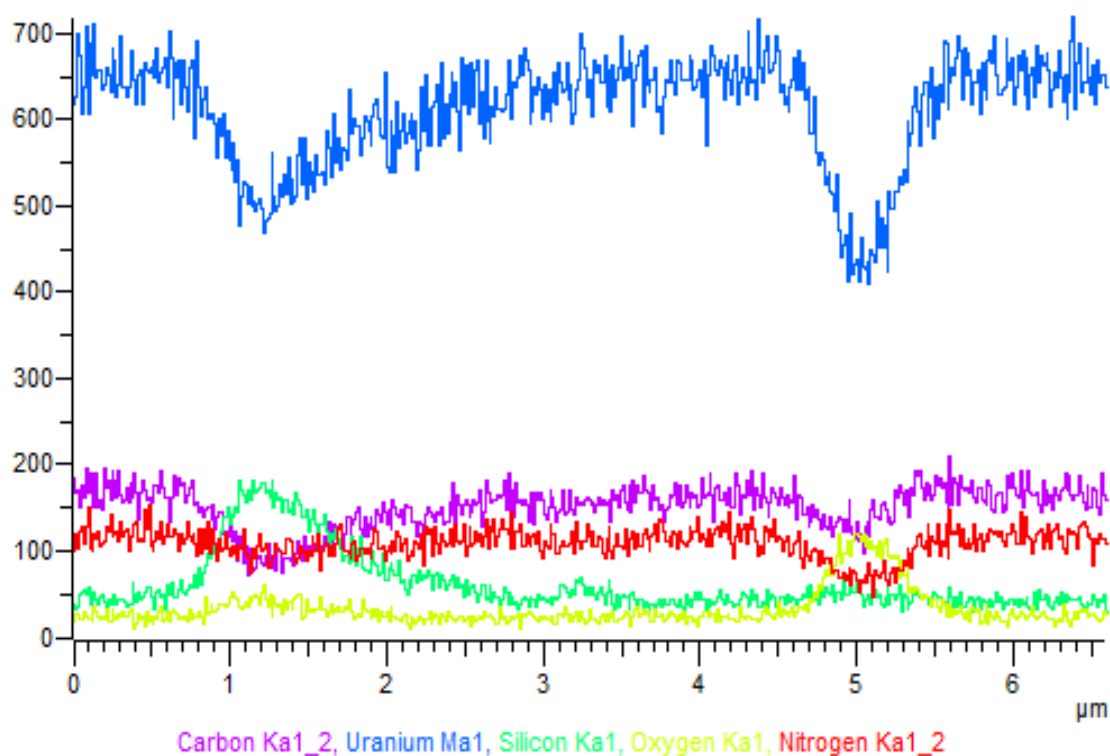


Figure 3.14: Obtained data from the line scan.

3.2.1.3 SUN150302A1

This pellet has a different sintering temperature (1450 °C) compared to the previous presented pellets, one could therefore assume a disparity in results. Analysis displayed that not a single needle-shaped phase was found. It would be a premature conclusion to say that it therefore does not exist at all in the pellet. But it gives a strong indication that at least it is more uncommon. Some of the silicon could be detected in cloud formed phases as seen in Figure 3.15-3.16. Line scan reveals a deep decrease of the uranium intensity and increase of oxygen which indicate that this is not anyone of the expected phases. Point scans exposed uranium and nitrogen in the bulk as expected and on the phase was trace elements like: Calcium, aluminium, fluorine, lanthanum, cerium, neodymium and iron found.

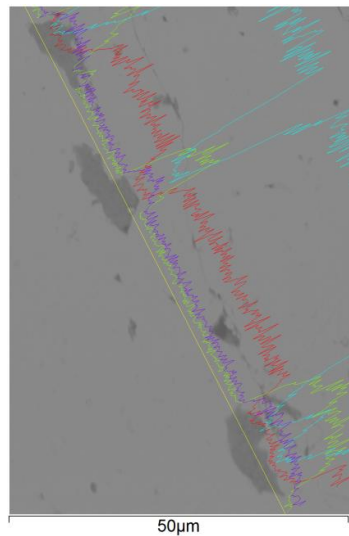


Figure 3.15: Line scan over cloud formed silicon phases in the SUN150302A5 pellet.

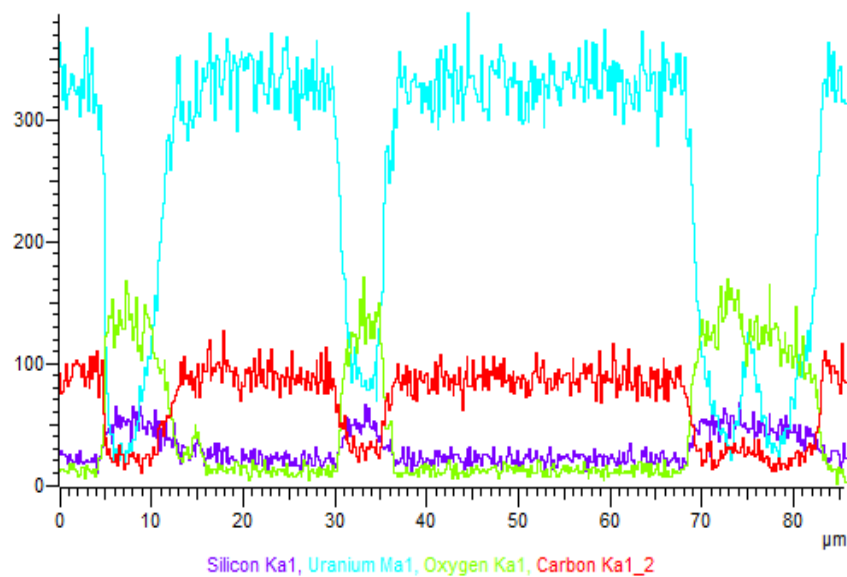


Figure 3.16: Obtained data from the line scan.

3.2.1.4 SUPD140331A1

The last examined pellet was also manufactured at 1450 °C but with the lower pressure during sintering. The needle-shaped silicide was hard to find in this pellet as well, but a found one can be seen in Figure 3.17-3.18. It seems to contain four different phases: a black & a white one, and two different grey colored. The line scan reveals a deep drop of uranium intensity and increase of silicon over the darker part of the grey colored phase. In the brighter grey an increase of oxygen is detected. Trace elements like molybdenum and tungsten also appears to be present. Results from five point scans can be seen in Table 3.1.

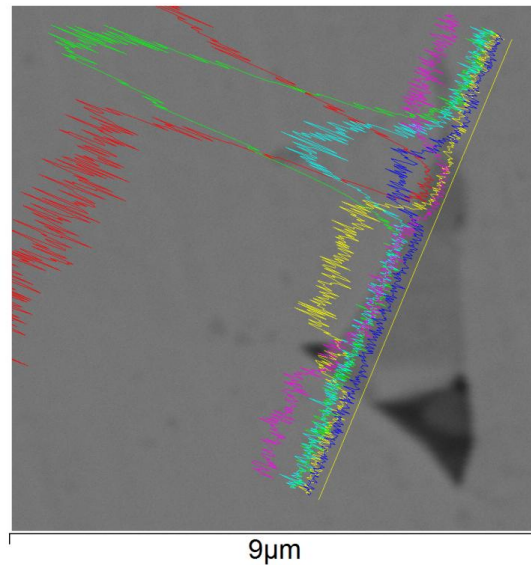


Figure 3.17: Line scan over a silicide in the SUPD140331A1 pellet.

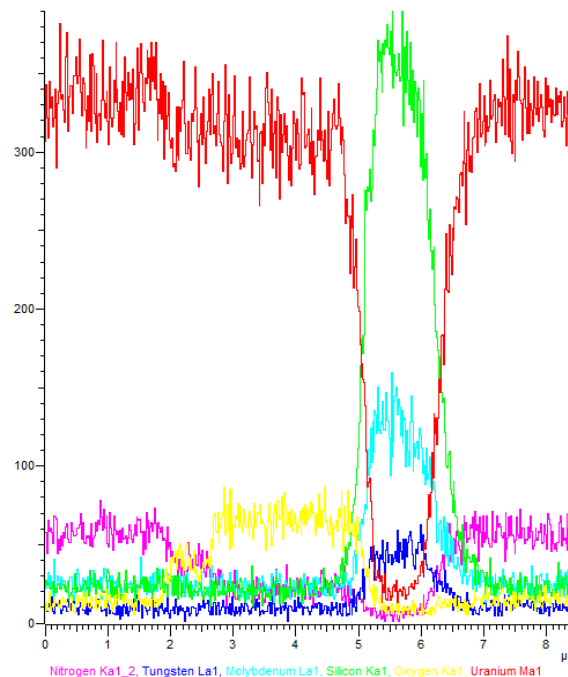


Figure 3.18: Obtained data from the line scan.

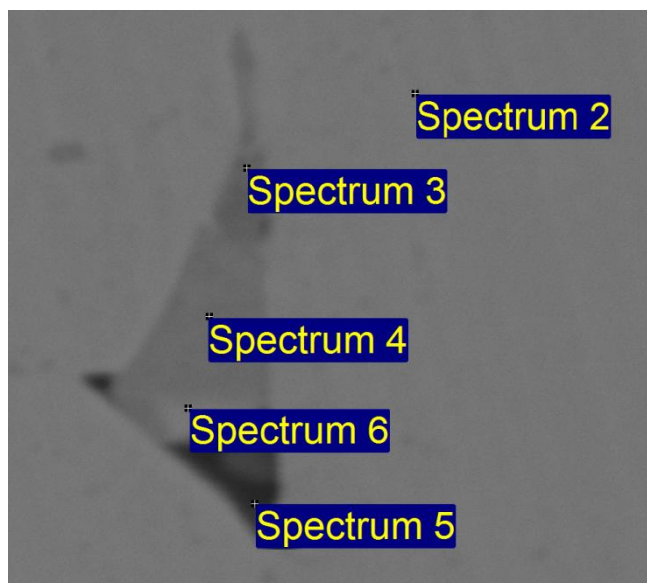


Figure 3.19: Five point scans on the silicide

Table 3.1: Obtained data from the point scans of the silicide containing four different phases.

Spectrum	C	N	O	Si	Ti	Fe	Ni	Mo	W	U	Total
Spectrum 2	10.05	16.98								72.97	100.00
Spectrum 3	16.16				1.49			19.21	63.14		100.00
Spectrum 4	12.13		14.00							73.87	100.00
Spectrum 5	12.27	6.91	5.20	1.18		5.93	2.35	16.68	3.54	45.95	100.00
Spectrum 6	11.82	9.21	5.13	0.81		1.81		4.32		66.88	100.00
Max.	16.16	16.98	14.00	1.18	1.49	5.93	2.35	19.21	63.14	73.87	
Min.	10.05	6.91	5.13	0.81	1.49	1.81	2.35	4.32	3.54	45.95	

All results in weight.%

Unexpectedly, spectrum 3 did not detect any silicon at all. Although the line scan suggest that this area should contain a large amount of it. This could be an indication that the SEM and its detector is not good enough for this analyse. A large amount of trace elements is also detected in the point scan.

3.2.1.5 Discussion

Results gathered to this point indicate a strong dependence of manufacturing variables during SPS and the silicon phase. Temperature appears to have the strongest influence as non or few needle-shaped silicides were found in pellets manufactured at 1450 °C. This observation is interesting since these pellets have a lower density compared to those that got manufactured at 1650 °C. This is kind of expected as a higher sintering temperature enables a shorter sintering time to achieve bonding between the powder particles, but, it is also a result which to some extent support the hypothesis that silicon acts as a pore filler.

Evaluating results from line and point scans are difficult since they are inconsistent. Uranium intensity change for pellets manufactured at 1650 °C suggest that U_3Si_5 and USi are the most likely phases. But values not corresponding to the expected phases are also common. This gives a hint that line scans might not be the optimal method to determine phases or that expected phases are inadequate. Line scans over the silicon phases in 1450 °C pellets reveals a vast drop of uranium intensity, indicating a completely different and unknown phase.

Point scans on the silicides in all pellets detected around ten trace elements. This result was unexpected as the majority of them was not detected in the XRF analysis. Because of this they were therefore often disregarded as limitations of the SEM, possible due to overlapping energy peaks. The result from scans also indicate a problem with the used SEM, as it appears to be of inferior quality for this type of analyse.

In the previous study [5], it was considered that the electrons emitted from the electron gun could penetrate the silicon phase and reach the uranium nitride phase beneath it, giving inaccurate result about the uranium concentration. This assumption followed into this thesis at an early stage, creating a source of concern as the results from EDS analyse might be unreliable. Later at KIMAB we got enlightened that the electrons do not penetrate the silicone phase. Since penetration depth for BSE is in the nm ($1 \cdot 10^{-9}$ m) scale. While the assumed spherical size of the silicide is in the μm ($1 \cdot 10^{-6}$ m) scale. But because of this concern combined with the inconsistent results, it was settled that to determine the silicon phase solely with EDS analyse would be too difficult. A decision was therefore taken to use solve a better SEM equipped with EBSD.

3.2.2 LEO 1530, Swerea KIMAB

As the thesis had a limited budget only the SUN150225A4 pellet got examined. The reason for selecting this pellet is that it appeared to have the highest amount of sought silicide phases.

Results

With a superior SEM, new EDS with an addition of EBSD analysis got produced. As the phase was going to be analysed using EBSD a final polishing was done using an etching agent (2% nital solution). This improves pattern quality by removing deformations emerged from grinding and polishing of the surface. Additionally, etching outlines the grain structure, which is an obvious benefit. An example on how the pellet appeared at a magnitude of 1000 can be seen in Figure 3.20.

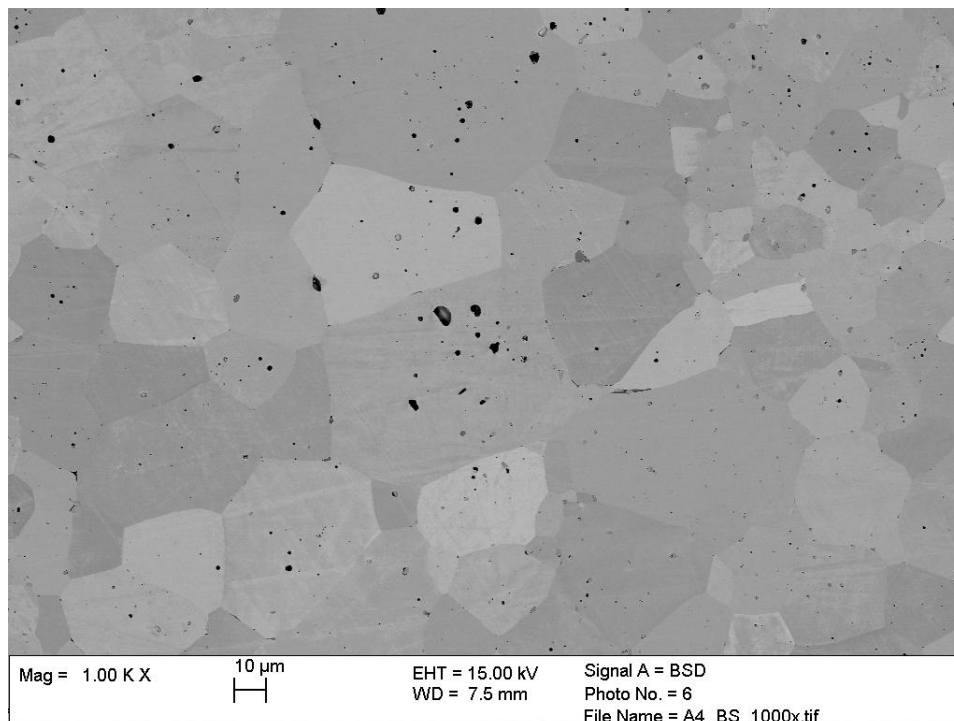


Figure 3.20: Pellet SUN150225A4 at Magnitude = 1000. Observe the now visible grain boundaries after etching with a 2% nital solution (ethanol and nitric acid)

3.2.2.1 EDS

An interesting region was found containing several different phases, see Figure 3.21. Ten point scans was performed with results summarised in Table 3.2. Considering the large amount of carbon, point scan number 2 is most likely detecting a pore. While the other nine point scans detect particles or the bulk.

Analysis of the bulk is shown in point scan number 10, with a result corresponding well to the XRF analyse. This is a good indicator that the microscope have a high accuracy. Point scan number 8 & 9 appears to be the sought phase. The results display a big difference between them as point scan number 8 have a higher amount of uranium and nitrogen, but lower amount of trace elements. This is very likely due to a mistake

when selecting area for point scan number 8. As it appears when zooming in that the silicide was not completely hit but rather slightly above.

With this knowledge, one could expect with a high probability that the two phases are the same with correct values from point scan 9.

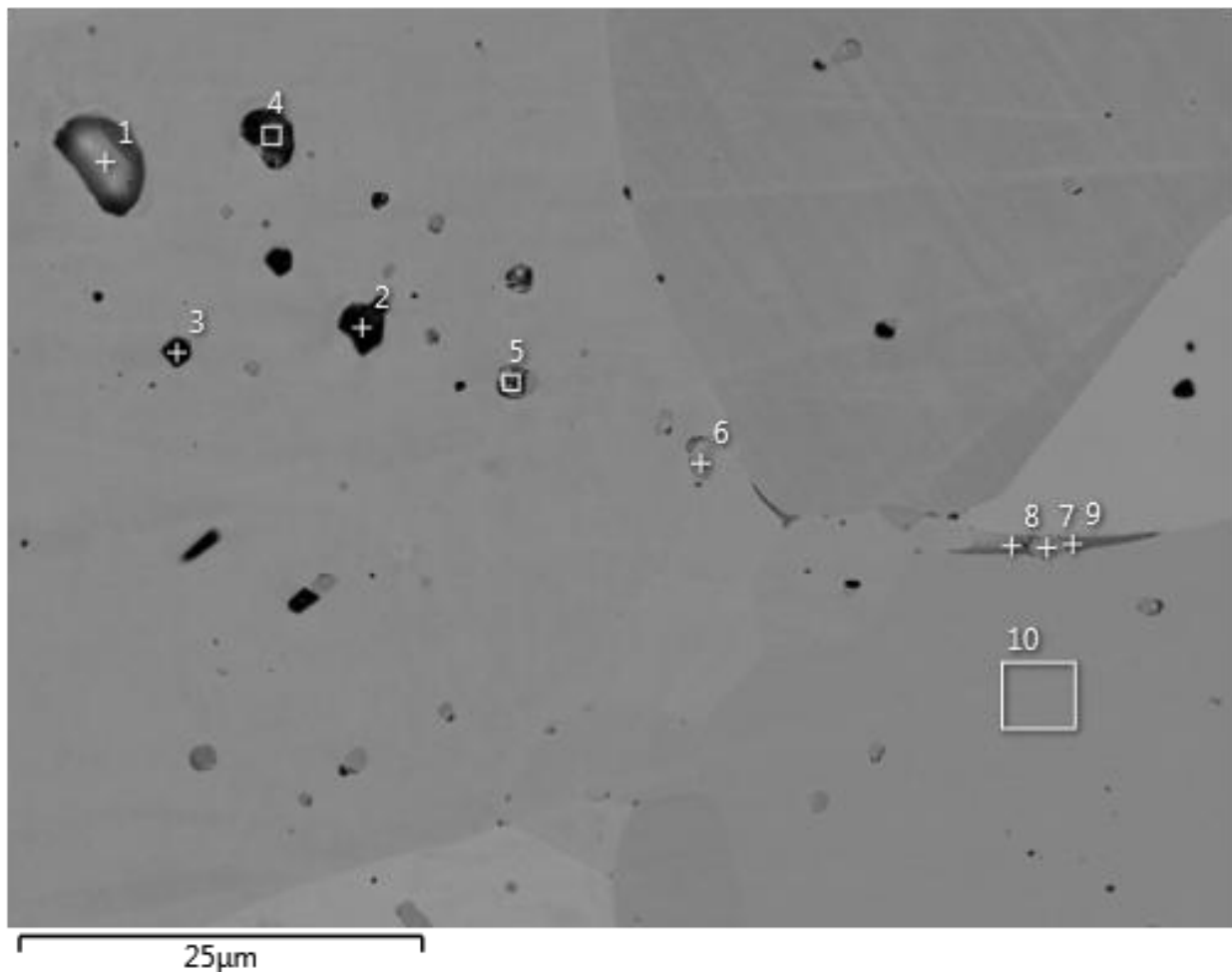


Figure 3.21: Ten point scans over an interesting region.

Another interesting result is the high amount of detected silicon found in point scan 3. This is a clear evidence that nor for pellets manufactured at 1650 °C or 1450 °C is silicon only gathered in needle-shaped phases. In fact, silicon is detected in every point scan. Observe from Table 3.1 that this was not detected with the previous SEM.

A total of 17 trace elements got detected, this is a similar phenomena to the one presented in section (3.2.1). Indicating that the decision to disregard them was incorrect.

Table 3.2: Data from ten point scans over an interesting region.

Element (wt.%)	1	2	3	4	5	6	7	8	9	10
C		36.52								
N	4.00				3.32	0.93	0.72	5.01	3.38	10.73
O	1.06	21.23	23.07	12.96	9.77	11.26	11.03	0.72	0.70	0.58
F		4.26	2.25	7.69	1.83		0.14			
Al		8.35		2.75	1.42					
Si	0.15	1.54	19.85	2.47	2.19	0.14	0.14	5.76	12.12	0.13
P			0.10	0.16						
S			0.20	0.15						
Cl		0.66	0.89	0.89	0.27					
Ca		0.30	0.62	1.86						
Cr								0.45	1.32	
Mn								0.10	0.44	
Fe		0.46	0.67	1.77				3.66	9.60	
Co								0.98	2.50	
Ni								0.67	1.69	
La		6.35	6.22	21.25	2.72					
Ce		9.29	9.62	29.72	4.57					
Pr		1.06	0.96	2.63	0.56					
Nd		2.63	2.62	7.14	0.80					
Sm			0.51	1.15						
U	94.80	7.36	32.42	7.42	72.55	87.67	88.10	82.65	68.25	88.57
Total:	100.00	100.00	100.00	100.00	100.00	100.00	100.00	100.00	100.00	100.00

Due to the etching, a remarkable discovery was made. The needle-shaped phase appears to be located nearly always at the grain boundary, frequently in close proximity to a 'chaotic' phase. The chaotic phase often consist of several different phases. An example of this can be seen in Figure 3.22 with results from point scans of the chaotic phase displayed in Table 3.3.

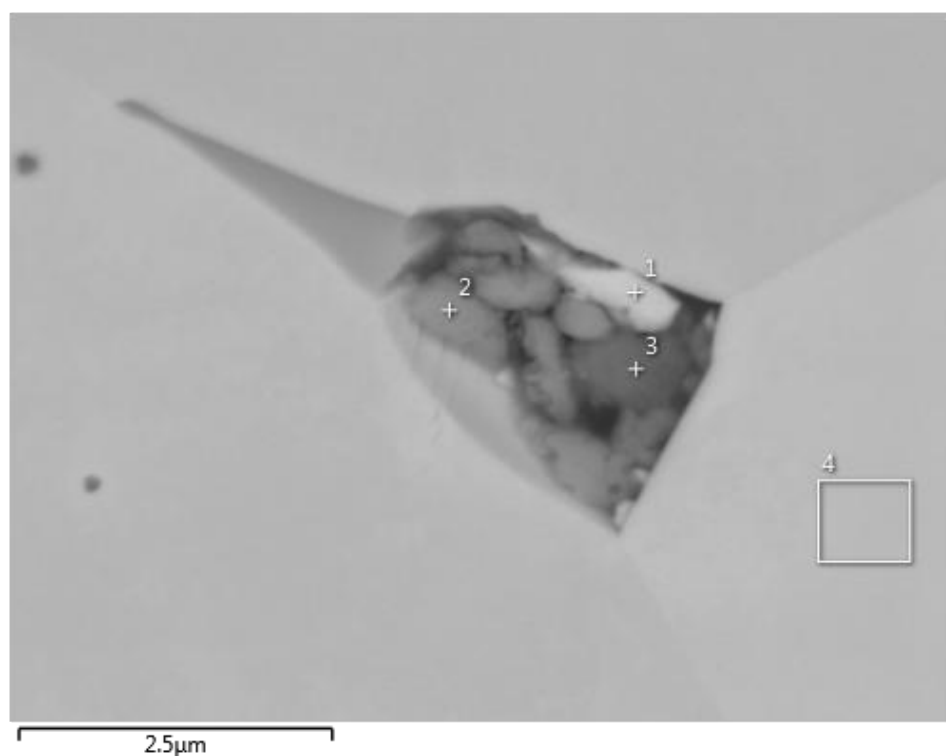


Figure 3.22: An needle-shape phase located at the grain boundary, in close proximity to a 'chaotic' phase. Three point scans over the chaotic phase was done.

Table 3.3: Data from point scans of the chaotic phase.

Element (wt.%)	1	2	3	4
N	8.76	1.33	0.85	10.28
O	2.85	13.66	12.45	0.38
F	0.26	1.89	0.84	
Si	0.37	3.97	1.30	0.10
S	0.19		4.93	
Fe		0.78		
Sr			1.94	
Ba			24.16	
La		18.03	4.34	
Ce	0.99	13.85	5.59	
Pr		2.07		
Nd		5.25		
U	86.57	39.17	43.60	89.24
Total:	100.00	100.00	100.00	100.00

Point scans on a silicide containing a darker phase on the tip was also performed, see Figure 3.23 & Table 3.4. Results are similar with previous observed ones, the brighter phase in point scan 1 contains nearly the same trace elements with equivalent amount as in point scan 9 seen in Table 3.2, with a small exception in the lack of manganese for this scan. The darker phase in point scan 3 contains several of the elements that got detected in the chaotic phase.

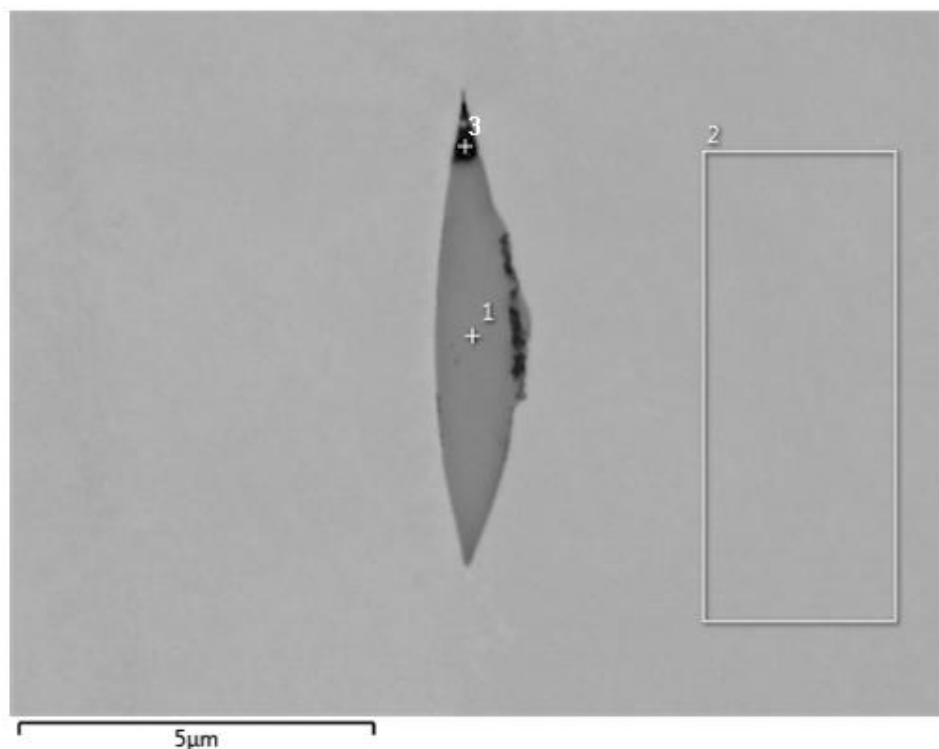


Figure 3.23: Point scans on a silicide containing a darker phase on the tip of it.

Table 3.4: Data from point scans of an silicide

Element (wt.%)	1	2	3
N	0.64	10.63	2.98
O	0.86		7.19
F			2.64
Si	16.36	0.11	4.1
Cr	1.3		
Co	3.02		
Ni	2.39		
Cl			0.71
Fe	12.09		1.64
La			5.9
Ce			9.43
Pr			0.62
Nd			1.9
U	63.34	89.26	62.89
Total:	100.00	100.00	100.00

3.2.2.2 EBSD

A few of the found needle-shaped phases got analysed using EBSD. For not a single one of them did the detected kikuchi lines match anyone of the expected phases. As an EBSD system needs to know which phases to index against in order to determine the most probable one, this became a problem.

Because of the large amount of detected trace elements in the EDS analyse, specifically: iron & cobalt. Phases containing these was added to the evaluation. Several of potential matching phases was now found. To be able to determine the correct one, a great amount of experience working with kikuchi patterns is needed. The used software AZtecEnergy also have an integrated function of calculating the Mean Angular Deviation (MAD). This is a number given in degrees which specify the averaged angular misfit between detected and simulated Kikuchi bands. The smaller the number, the better the match, values less than 1° is acceptable for most systems [21].

All the analyses displayed the same outcome. Result from one of them can be seen in Figure 3.24, it appears that the needle-shaped phase in this pellet is: **(Co₃Si₅U₂)**. But, since the magnetic trace elements (iron, nickel, molybdenum, manganese, etc) easily could substitute the cobalt. It is most likely a phase structure consisting of **(X_xSi_xU_x)**

3.2.2.3 Discussion

Interpreting results gathered from this analyse is more straightforward compared to previous one, due to the better SEM. A major discovery is that the silicide is nearly-always located at the grain boundary. This indicate that during the SPS process, silicon together with all the other detected trace elements is being pushed out from the bulk towards the grain boundaries. A result which falsify the theory of silicon acting as a pore filler, but rather is creating pores between grains as it is ejected from the bulk.

Another interesting result is that silicon is detected in all particles and not (as previously thought) primarily in the needle-shape phase. In fact, the majority of the silicon is located in the bulk as the concentration there lies between 0.10-0.13 wt.%. This feature was not detected in point scans during the previous analyse, though there is signs of it in line scans graph.

As silicon was identified in the bulk it was assumed to be dissolved substitutionally in the nitrogen lattice. In an earlier study [22], the solubility limit of silicon in UN at 1500 °C got estimated to (UN_{0.72}Si_{0.28}) with a lattice parameter of 4.9003 Å. Since the examined pellet only contains around (UN_{0.991}Si_{0.09}) silicon, there is no surprise that we do not observe a shift of the lattice parameter in the bulk.

Combining these discoveries makes it fairly safe to say that, the impact on density from silicon impurities is negligible in the SUN150225A4 pellet. As this was the only pellet that got examined, it is not certain that this result applies to the other pellets. But since the only difference is the SPS parameters which should not affect this type of result, and nothing in the analyses indicate a difference, it is very likely that the same phenomena apply in the other pellets. Confirmation of this could be an interesting point to continue from for future studies.

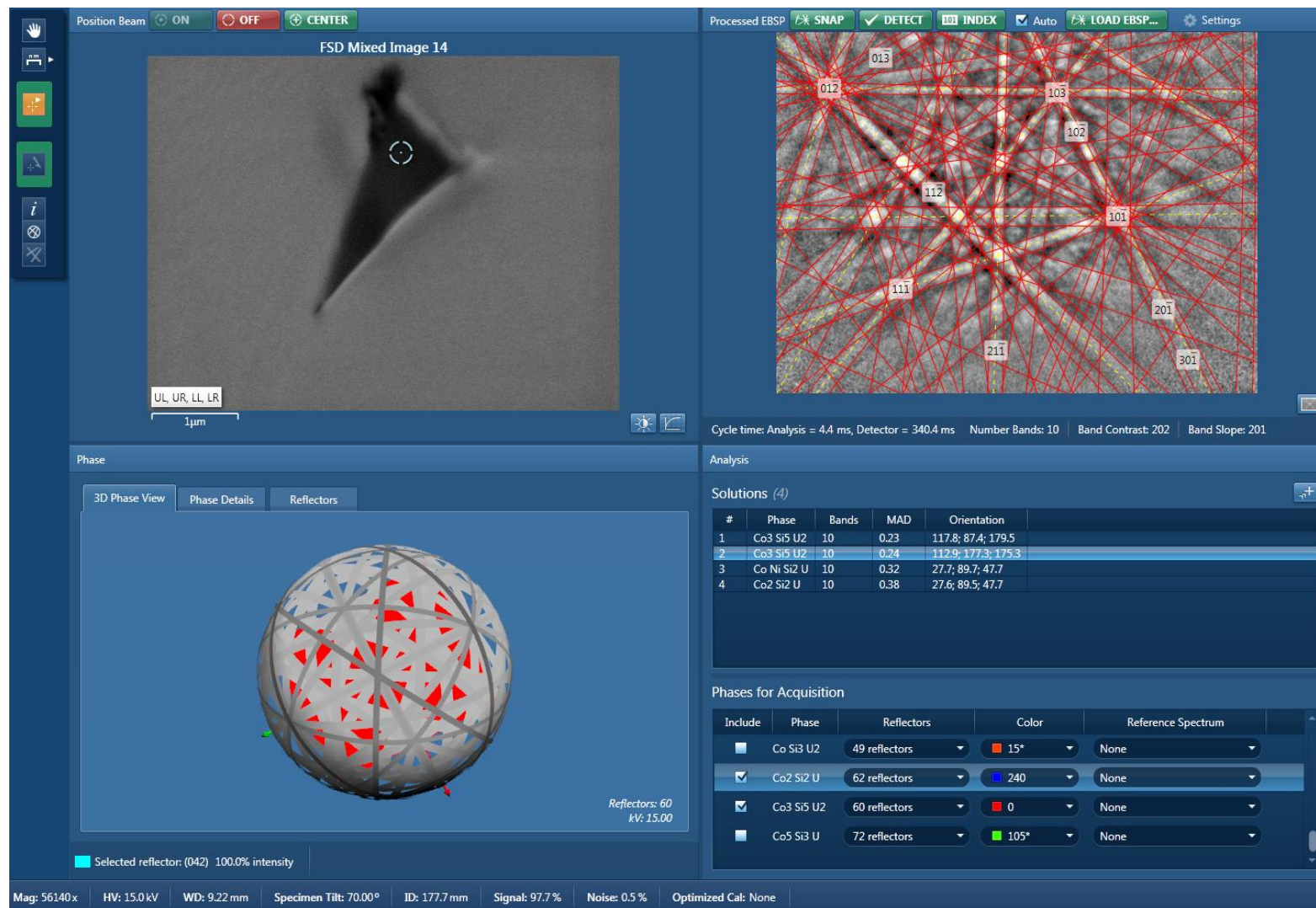


Figure 3.24: Interface of the AZtecEnergy software. To the upper left is the observed silicide and right to it is the kikuchi pattern. Below this pattern is the integrated MAD function, which display that Co3Si5U2 is the most likely phase.

4. Conclusion

A new manufacturing method able to synthesis uranium nitride pellets close to fully dense, has been the subject of this thesis. During the synthesis process, silicon arise in pellets as an impurity due to contamination from a quartz filter. In previous studies it was assumed that most of this silicon settles in pores as needle-shapes during spark plasma sintering, thereby increasing density. Depending on which phase the silicon is in the increase can vary. Exact impact of this has to be evaluated in order to permit assessment of measured thermal conductivity of the pellets [3].

The aim of this thesis has been to analyse these pellets and identify the silicon phases using a SEM. It is a continuation from a previous research that tried to solve it by using an EDS detector to analyse elemental composition. The method utilised that intensity of the signal strength is proportional to amount of the element [5]. By analysing the uranium intensity in the bulk and compare it with the silicides, one should be able to estimate the phase. This method was also attempted in this thesis with deficient and inconsistent results. A decision was therefore taken to use a better SEM equipped with an EBSD detector.

These analysis revealed that the starting assumptions for this and previous studies has been incorrect. The concentration of silicon in the bulk is around 0.10-0.13 wt.%, this is almost the total amount of it in the pellets according to XRF analysis. A result which falsify the assumption of silicon mainly being located inside the silicide phases. Another discovery was that the silicide phases are nearly-always located at the grain boundary, together with a large spectrum of trace elements. This discovery falsify the theory of silicon acting as a pore filler. A more reasonable explanation is that during the SPS process, silicon together with the other detected trace elements gets pushed out from the bulk towards the grain boundaries, where it forms different particles and phases. Using EBSD the needle-shape phase got determined to $(\text{Co}_3\text{Si}_5\text{U}_2)$ in one of the pellets. But due to possible substitution of the cobalt with any detected magnetic trace element, it is more likely a $(\text{X}_x\text{Si}_x\text{U}_x)$ phase.

The consequence of these results is that the impact on density from the needle-shape phase and other silicon phases is negligible. Compared to previous published results, the reliability is higher in this thesis as more data got collected and a superior SEM was used. Due to a limited budget only one pellet got examined with EBSD, it is therefore still uncertain if pellets with different SPS manufacturing parameters contains the same silicon phases. But since nothing indicate that the same phenomena of silicon being negligible, would not apply in these pellets. No further investigations was done on this subject.

5. References

- [1] The Generation IV International Forum (GIF)
Website: https://www.gen-4.org/gif/jcms/c_9260/public , 06/30/2015
- [2] World Nuclear Association - Generation IV Nuclear Reactors
Website: <http://www.world-nuclear.org/info/Nuclear-Fuel-Cycle/Power-Reactors/Generation-IV-Nuclear-Reactors/> , 06/30/2015
- [3] P. Malkki, M. Jolkkonen, T. Hollmer and J. Wallenius.
Manufacture of fully dense uranium nitride pellets using hydride derived powders with spark plasma sintering.
Journal of Nuclear Materials, 2014. Volume 452, Issues 1–3, pp 548–551
- [4] S.L. Hayes, J.K. Thomas, K.L. Peddicord
Material property correlations for uranium mononitride IV. Thermodynamic properties.
Journal of Nuclear Materials, 1990. Volume 171, Issues 2–3, pp 289–299
- [5] V. Schamböck.
Analysis of silicon phases in highly dense uranium nitride pellets.
Project Work, 2015
- [6] T. Muromura, H. Tagawa,
Formation of uranium mononitride by the reaction of uranium dioxide with carbon in ammonia and a mixture of hydrogen and nitrogen - Synthesis of high purity UN.
Journal of Nuclear Materials, 1977. Volume 71, Issue 1, pp 65–67
- [7] H. Muta, K. Kurosaki, M. Uno, S. Yamanaka.
Thermal and mechanical properties of uranium nitride prepared by SPS technique
Journal of Materials Science, 2008. Volume 43, Issue 19, pp 6429–6434
- [8] T. Hollmer
Manufacturing methods for (U-Zr)N-fuels
Diploma thesis, 2011
- [9] George F. Vander Voort
Specimen Preparation for Image Analysis
Practical Guide to Image analysis, ASM International, 2000, Chapter 3,

- [10] Y. Lang
Scanning Electron Microscope
Materials Characterization, John Wiley & Sons, 2008, Chapter 4, pp.127-161,
- [11] SEAL Laboratories
How SEM Works
Website: <http://www.seallabs.com/how-sem-works.html>
- [12] The MicroAnalytical Facility
Digital Imaging and Mapping
Website: http://epmalab.uoregon.edu/pdfs/Mapping2%20Chap%208_.pdf
- [13] S. Amelinckx, D. van Dyck, J. van Landuyt, G. van Tendeloo
Scanning Beam Methods
Handbook of Microscopy: Applications in Materials Science, Solid-State Physics and Chemistry Applications, Methods II, Wiley-VCH, 2008, Chapter 2, pp.537-561
- [14] D.Brandon, W.D Kaplan
Scanning Electron Microscopy
Microstructural Characterization of Materials - 2nd Edition, John Wiley & Sons, 2008, Chapter 5, pp.261-331
- [15] Y.Lang
X-ray Spectroscopy for Elemental Analysis
Materials Characterization : Introduction to Microscopic and Spectroscopic Methods, John Wiley & Sons, 2009, Chapter 6, pp.171-196
- [16] T.Maitland, S.Sitzman
Electron Backscatter Diffraction (EBSD) Technique and Materials Characterization Examples
Scanning Microscopy for Nanotechnology: Techniques and Applications, Springer, 2009, Chapter 2, pp.41-75
- [17] Web Elements
Website: <http://www.webelements.com/>
- [18] Yeon Soo Kim
Uranium Intermetallic Fuels (U-Al, U-Si, U-Mo)
Comprehensive Nuclear Materials, Chapter 3.14, p.402
- [19] Geochemical Instrumentation and Analysis
X-Ray Fluorescence (XRF)
http://serc.carleton.edu/research_education/geochemsheets/techniques/XRF.html

- [20] Geochemical Instrumentation and Analysis
X-ray Powder Diffraction (XRD)
http://serc.carleton.edu/research_education/geochemsheets/techniques/XRD.html
- [21] Oxford Instrument
AZtec User Manual
Issue 2.1, 2013, p.446
- [22] S. Imoto, K. Niihara, H. -J. Stöcker
Thermodynamics of nuclear materials. Solid solubility in NaCl-type uranium compounds
International Atomic Energy Agency, Vienna, 1968